Performance Analysis of Cooperative Aerial Base Station-Assisted Networks with Non-Orthogonal Multiple Access

Xianling Wang, *Member, IEEE,* Haijun Zhang, *Senior Member, IEEE,* Kyeong Jin Kim, *Senior Member, IEEE,* Yue Tian, *Member, IEEE,* and Arumugam Nallanathan, *Fellow, IEEE*

Abstract

The use of aerial base stations (ABSs) is gaining attention due to its potentials to provide a flexible wireless coverage in adverse scenarios. Investigations on key performance metrics are desirable to ensure the feasibility of these ABS-assisted networks, especially when they are jointly designed with advanced transmission technologies, e.g., cooperative transmissions and non-orthogonal multiple access (NOMA). In this paper, we consider an ABS-assisted cooperative system with NOMA enabled to boost connectivity ability. It is assumed that multiple ABSs hover around a macro base station to relay downlink signals to user equipments, while interfering nodes are randomly distributed on the ground. We assume a more realistic channel model featured with a distance-related probabilistic line-of-sight and non-line-of-sight propagation, as well as non-identical small-scale fading. We derive the outage probability, and study the impacts of various parameters on the system performance. Numerical results unveil that: 1) The reliability of backhauls plays an important role in the system and determines the outage performance floor. 2) Joint transmissions from the sky can bring in a significant performance enhancement for the

X. Wang and Y. Tian are with Fujian Key Laboratory of Communication Network and Information Processing, Xiamen University of Technology, Xiamen 361024, China (e-mail: xianling.wang@ieee.org; yue.tian.xmut@outlook.com).

H. Zhang is with Beijing Advanced Innovation Center for Materials Genome Engineering, Beijing Engineering and Technology Research Center for Convergence Networks and Ubiquitous Services, the University of Science and Technology Beijing, Beijing 100083, China (e-mail: haijunzhang@ieee.org).

K. J. Kim is with Mitsubishi Electric Research Laboratories (MERL), Cambridge, MA 02139, USA (e-mail:kkim@merl.com).

A. Nallanathan is with the School of Electronic Engineering and Computer Science, Queen Mary University of London, London E1 4NS, U.K. (e-mail:nallanathan@ieee.org).

Manuscript received April 3, 2019; revised April 3, 2019.

system. 3) The NOMA based transmission outperforms the traditional orthogonal multiple access with an improved outage performance, provided a properly selected NOMA power allocation coefficient.

Index Terms

Aerial base station, cooperative communication, line-of-sight/non-line-of-sight propagation, non-coherent joint transmission, non-orthogonal multiple access, stochastic geometry.

I. Introduction

In recent years, we have witnessed a rapid proliferation of unmanned aerial vehicles (UAVs) in all areas due to the advance in their payload capacity and prolonged battery life [1]. In wireless communications, with low-cost wireless tranceivers mounted, the UAVs are envisioned as bringing in a paradigm shift for next generation networks [2], [3]. Compared with terrestrial base stations (BSs), UAV-mounted aerial base stations (ABSs) present more effective solutions to overcome propagation constraints and realize seamless coverage in adverse scenarios (e.g., disasters, equipment failures, and rough topography) [4]. Besides, the ABSs can also find their applications in cutting-edge network architectures, such as ultra dense networks to facilitate traffic offloading [5], [6], and mobile edge networks to assist caching and computing [7].

Meanwhile, driven by the unprecedented increase in user demand, researchers from industrial and academia are also focused on advanced transmission technologies, such as cooperative transmissions [8], [9] and non-orthogonal multiple access (NOMA) [10], [11]. In cooperative transmissions, multiple BSs communicate with each other and jointly transmit signals concurrently, leading to an improved cell edge coverage performance. In NOMA, the signals of different users are multiplexed on the same resource block, enhancing the ability to support massive connections. Given the considerable performance gain, incorporating above technologies into ABS-assisted networks will be of great significance and investigations on the key performance metrics are desirable.

A. Related Works and Motivation

The ABS-assisted communication systems take several advantages. On one hand, transmitting radio signals from the sky offers communication channels dominated by line-of-sight (LoS) links, which produce a better received signal quality than non-line-of-sight (NLoS) links. Some researchers have studied the impacts of LoS link propagation on the ABS-assisted networks.

Based on the binomial point process (BPP) model, the authors in [12] considered offloading traffic from the macro base station (MBS) tier to the ABS tier and investigated the impacts of a more realistic probabilistic LoS propagation model on the system performance. The high possibility of LoS link has also promoted the applications of millimeter wave (mmWave) transmissions in ABS-assisted networks [13], [14]. The work in [13] investigated the limitations of physical vertical beamwidth of mmWave transmissions and proposed a beam scanning approach for the ABS-assisted network to maximize the achievable rate. In [14], the authors explored the 3D antenna gain for the mmWave transmission in the ABS-assisted network and proposed a transmit jamming strategy to improve the secrecy performance.

On the other hand, the mobility of ABSs enables a new framework to improve the system performance through deployment and trajectory optimizations. In [15], the authors jointly optimized the placement and mobility of the ABSs to provide reliable and energy efficient uplink communications for internet of things (IoT). In [16], the authors proposed an efficient successive ABS placement algorithm to achieve wireless connectivity with a minimum number of ABSs. The authors in [17] considered ABS's trajectory as a new design dimension to realize energy efficient ABS communications.

Recently, in the backdrop of ultra dense networking, cooperative communications [18], [19] and NOMA [20], [21] have also been studied extensively. The performance gain brought in by these technologies has driven joint designs with the ABSs. In [22], the authors compared the outage and bit error rate performance of two typical use cases, i.e., the multi-hop single link scheme and the multiple dual-hop links scheme, and unveiled useful design guidelines for a multi-ABS based relay system. In [23], a novel clustering scheme was proposed, in which partially energy-harvesting-powered ABSs cooperatively offload users' traffic for the terrestrial cellular networks. In [24], the authors proposed a novel architecture of joint transmission in the cognitive satellite-terrestrial network associated with an ABS. The work in [13] considered a NOMA based ABS-assisted network, in which users within the mmWave beam direction were paired to improve connectivity. The authors in [25] applied NOMA to enhance the capacity of wireless backhauls. They further maximized the sum achievable rate of all users by jointly determining the resource allocation, NOMA decoding order, and ABS positions. In [26], a novel cooperative NOMA scheme was proposed to mitigate the uplink interference without significantly compromising the achievable rate for a ABS-assisted network.

Inspired by the great potential illustrated in [22], [23], [25], in this paper, we incorporate coop-

erative communications and NOMA into ABS-assisted networks. To the best of our knowledge, few effort has been put in this context, especially under the probabilistic LoS propagation and non-identical small-scale fading condition. The authors in [27] considered a similar mathematical model, however their work was mainly focused on the terrestrial system, which neglected the probabilistic LoS propagation feature of the ABSs. Besides, NOMA based transmissions and PPP based interference modeling were not taken into consideration in [27]. Part of the investigation was published in [28], and this work extends [28] in following ways: 1) The deterministic LoS propagation model is extended to a probabilistic LoS propagation model for air-to-ground channels. 2) NOMA is considered in this work, where multiple ABSs jointly transmit superimposed signals to more than one users. 3) This paper provides enriched studies on the impacts of system parameters on the performance metrics.

B. Contributions

The main contributions of the paper are summarized as follows.

1) Modeling of the Cooperative ABS-Assisted Networks with Non-Coherent Joint Transmission and NOMA: We develop a general analytical framework to study the system performance of the ABS-assisted network with non-coherent joint transmissions (NC-JT) and NOMA. To be specific, multiple ABSs are deployed around the MBS and relay the downlink signals to user equipments (UEs) through wireless backhauls and wireless accesses. NOMA is applied to realize simultaneous signal transmissions on a single resource block for different UEs. Multiple active ABSs forward the superimposed signal through NC-JT to allow a coherent power combination at different UEs. We integrate the probabilistic LoS and NLoS propagation model, as well as non-identical Nakagami-m fading, which requires tools from combinatorics and complicates the analysis. We also consider PPP based interfering nodes and resort to stochastic geometry to deal with the aggregate interference. Then, exact expressions for outage probabilities are provided to enable numerical evaluation on the system performance.

2) System Design Guidelines: We investigate the impacts of different parameters including unreliable wireless backhaul, ABS number, and ABS height based on the new developed analytical framework. It is revealed that the reliability of wireless backhauls will determine the outage probability floor. However, this constraint can be compensated by joint transmissions with multiple ABSs, and hence brings in a lower system outage probability and higher outage sum rate. Another observation is that under the probabilistic LoS propagation model, the ABS

height should be carefully designed to achieve the lowest outage probability. This optimal height balances the positive impact of increased LoS probability and the negative impact of stretched communication distances. Besides, the system performance are also influenced by the fading parameters and the target rates.

3) Comparison with the Orthogonal Multiple Access Scheme: We also investigate the superiority of the NOMA scheme over the traditional orthogonal multiple access (OMA) scheme in terms of the outage probability, outage sum rate, and energy efficiency. Our study shows that, an improvement in the outage probability over the OMA scheme can be expected by applying the NOMA scheme. This improvement can be achieved by properly selecting the NOMA power allocation coefficient, and is more obvious when the lower priority user requires higher target rates.

The rest of the paper is organized as follows. In Section II, we describe the considered ABS-assisted network model and transmission schemes. In Section III, we analyze the statistical characteristics for the received signals at the ABSs and the UEs. In Section IV, we derive the outage probabilities for the two transmission phases, respectively. Section V validates our analytical expressions and provides discussions on the observations obtained through computer simulation. Finally, conclusions are drawn in Section VI.

II. System Model

A. Network Model

We consider a downlink ABS-assisted single-antenna network including one MBS, two user equipments (UEs), and a set of K ABSs denoted by $\mathbf{b}$, $\{\mathbf{u}_1, \mathbf{u}_2\}$, and $\mathcal{R} = \{\mathbf{r}_1, \cdots, \mathbf{r}_k, \cdots, \mathbf{r}_K\}$, respectively. Assume that co-channel interfering nodes are randomly distributed in the whole 2D plane $\mathbb{R}^2$, forming a PPP denoted by $\Phi = \{\mathbf{z}_i, i \in \mathbb{N}^+\}$ with density λ. Set the location of $\mathbf{b}$ as the origin $\mathbf{o}$ of the coordinates. With a slight abuse of notation, we also use $\mathbf{b}$, $\mathbf{u}_j$ ($j \in \{1, 2\}$), $\mathbf{r}_k$, and $\mathbf{z}_i$ to denote the coordinates of these nodes. The transmit power of $\mathbf{b}$, $\mathbf{r}_k$, and $\mathbf{z}_i$ are $P_{\mathbf{b}}$, $P_{\mathbf{r}}$, and $P_{\mathbf{z}}$, respectively. For simplicity, we assume that all ABSs statically hover around $\mathbf{b}$ at the same height h, and the locations of the ABSs and the UEs are deterministic.

Assume that, due to severe shadowing, no direct communication link exists between $\mathbf{b}$ and $\mathbf{u}_j$. This can also be the result of the closed access policy or pre-determined agreement between the network operator and the users. Therefore, the downlink service for $\mathbf{u}_j$ relies on the ABSs in $\mathcal{R}$, which retrieve data signals from $\mathbf{b}$. We term wireless backhaul and wireless access to

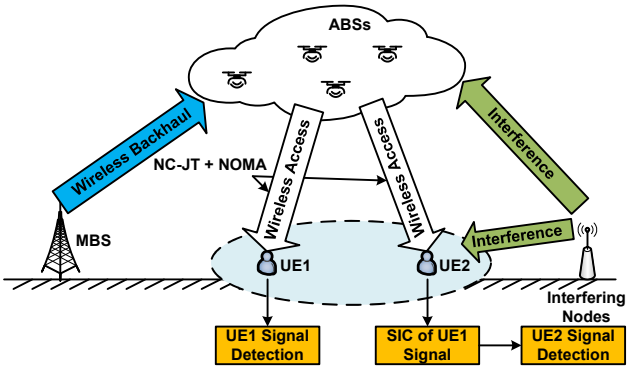

Fig. 1. Network architecture of the ABS-assisted network: 1) ABSs receive users' data through wireless backhauls from the MBS, and then provide wireless accesses for $\mathbf{u}_1$ and $\mathbf{u}_2$ through NC-JT and NOMA. 2) The signals for $\mathbf{u}_1$ are assigned more power, hence SIC is activated at $\mathbf{u}_2$ to remove inter-user interference. 3) Both wireless backhauls and wireless accesses are disturbed by interfering nodes.

differentiate the link from $\mathbf{b}$ to the ABSs, and that from the ABSs to the UEs. An example of the considered network model is illustrated in Fig. 1.

B. Channel Model

Let $\tilde{D}_k$, $D_{k,j}$, $\tilde{Z}_{i,k}$, and $Z_{i,j}$ be the distances from $\mathbf{b}$ to $\mathbf{r}_k$, from $\mathbf{r}_k$ to $\mathbf{u}_j$, and from $\mathbf{z}_i$ to $\mathbf{r}_k$ and $\mathbf{u}_j$, respectively. Then, as shown in Fig. 2, the communication system involves air-to-ground (A2G) channels and ground-to-ground (G2G) channels. We apply distance-dependent probabilistic LoS propagation models. Under this model, radio signal attenuation probabilistically follows LoS propagation with a lower path-loss exponent and Nakagami-m small-scale fading, or NLoS propagation with a higher path-loss exponent and Rayleigh small-scale fading.

1) A2G Channel: The ABS-assisted network takes the advantage of a higher chance to avoid blockage by transmitting signals through A2G channels, which apply to the wireless backhauls, e.g., from $\mathbf{b}$ to $\mathbf{r}_k$, the wireless accesses, e.g., from $\mathbf{r}_k$ to $\mathbf{u}_j$, and the interference links between the interfering nodes and the ABSs, e.g., from $\mathbf{z}_i$ to $\mathbf{r}_k$. To facilitate analysis, we resort to the channel model applied in [12] to calculate the occurrence probability of LoS A2G link. Let ϕ be the elevation angle, which is calculated in degree, from a ground terminal to an ABS. Then, the occurrence probabilities of LoS and NLoS links are determined by

$$\mathrm{P}_{\mathrm{AL}}(\phi) = \frac{1}{1 + c\exp(-b(\phi - c))} \quad \text{and} \quad \mathrm{P}_{\mathrm{AN}}(\phi) = 1 - \mathrm{P}_{\mathrm{AL}}(\phi), \tag{1}$$

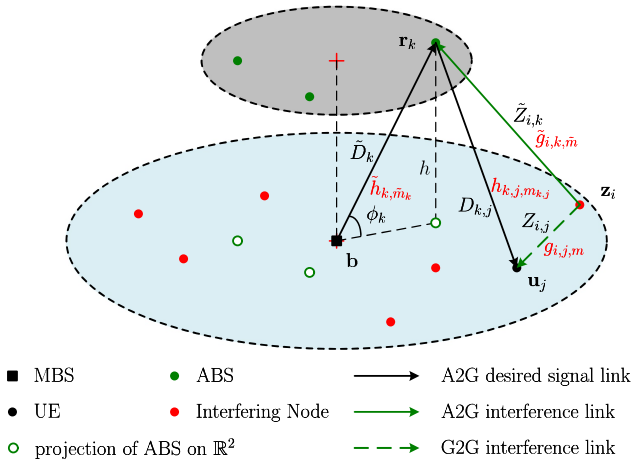

Fig. 2. Illustration of the distances and small-scale fadings: 1) $\tilde{D}_k$, $D_{k,j}$, $\tilde{Z}_{i,k}$, and $Z_{i,j}$ in black are the distances from $\mathbf{b}$ to $\mathbf{r}_k$, from $\mathbf{r}_k$ to $\mathbf{u}_j$, and from $\mathbf{z}_i$ to $\mathbf{r}_k$ and $\mathbf{u}_j$, respectively. 2) $\tilde{h}_{k,\tilde{m}_k}$, $h_{k,j,m_{k,j}}$, $\tilde{g}_{i,k,\tilde{m}}$, and $g_{i,j,m}$ in red are the small-scale channel power gains for the links from $\mathbf{b}$ to $\mathbf{r}_k$, from $\mathbf{r}_k$ to $\mathbf{u}_j$, and from $\mathbf{z}_i$ to $\mathbf{r}_k$ and $\mathbf{u}_j$, respectively.

where b and c are constant values depending on environments. It is revealed in (1) that with a larger elevation angle, the radio signal transmission is more likely to experience the LoS propagation, which is in line with reality. Note that in the practical scenario, the wireless backhaul may not be symmetric to the wireless access due to open area deployment of the MBS as surveyed in [29]. However, in the dense urban scenario, $\mathbf{b}$ may also be a small cell base station, which is easily blocked by buildings. In this case, the ground-to-air link may also be full of scatters, so that applying (1) to determine the LoS probability is still reasonable. As shown in Fig. 2, for the link between $\mathbf{b}$ and $\mathbf{r}_k$, the elevation angle can be calculated as $\phi_k = \arcsin\left(\frac{h}{\tilde{D}_k}\right)$. For simplicity, we rewrite the occurrence probabilities in (1) as the functions of the distance between the transmitter and receiver, e.g., $\mathrm{P}_{\mathrm{AL}}\left(\tilde{D}_k\right)$, given that all ABSs hovers at the same height h.

Denote by $\zeta_{\mathbf{b},\mathbf{r}_k}$, $\zeta_{\mathbf{r}_k,\mathbf{u}_j}$, and $\zeta_{\mathbf{z}_i,\mathbf{r}_k}$ the channel power gain from $\mathbf{b}$ to $\mathbf{r}_k$, from $\mathbf{r}_k$ to $\mathbf{u}_j$, and from $\mathbf{z}_i$ to $\mathbf{r}_k$, respectively. It is assumed that the path-loss exponents α_{L} and α_{N} $(2 < \alpha_{\mathrm{L}} < \alpha_{\mathrm{N}})$ for LoS and NLoS propagation is represented by α. Then, taking both path-loss and small-scale fading into account, we have

$$\zeta_{\mathbf{b},\mathbf{r}_k} = \tilde{D}_k^{-\alpha}\tilde{h}_{k,\tilde{m}_k}, \quad \zeta_{\mathbf{r}_k,\mathbf{u}_j} = D_{k,j}^{-\alpha}h_{k,j,m_{k,j}}, \quad \text{and} \quad \zeta_{\mathbf{z}_i,\mathbf{r}_k} = \tilde{Z}_{i,k}^{-\alpha}\tilde{g}_{i,k,\tilde{m}}, \tag{2}$$

where $\tilde{h}_{k,\tilde{m}_k}$, $h_{k,j,m_{k,j}}$, and $\tilde{g}_{i,k,\tilde{m}}$ are the small-scale channel power gains from $\mathbf{b}$ to $\mathbf{r}_k$, from $\mathbf{r}_k$ to $\mathbf{u}_j$, and from $\mathbf{z}_i$ to $\mathbf{r}_k$, respectively. Upon applying the Nakagami-m fading assumption for the LoS propagation, $\tilde{h}_{k,\tilde{m}_k}$, $h_{k,j,m_{k,j}}$, and $\tilde{g}_{i,k,\tilde{m}}$ are independently gamma distributed with shape

parameters $\tilde{m}_k \in \mathbb{N}^+$, $m_{k,j} \in \mathbb{N}^+$, and $\tilde{m} \in \mathbb{N}^+$, and scale parameters $1/\tilde{m}_k$, $1/m_{k,j}$, and $1/\tilde{m}$.[1] Note that we consider non-identical Nakagami-m fading for the desired signal links, i.e., $\tilde{h}_{k,\tilde{m}_k}$ and $h_{k,j,m_{k,j}}$, which are reflected by the variations in $\tilde{m}_k$ and $m_{k,j}$ for different k and j. As for the interference links from $\mathbf{z}_i$ to $\mathbf{r}_k$, identical Nakagami-m fading with a fixed $\tilde{m}$ is adopted for simplicity. Also note that, by setting the shape and scale parameters to be 1, the gamma distributed random variable naturally degrades to be exponentially distributed, yielding Rayleigh fading for the NLoS propagation.

It should be noted that, the LoS propagation probabilities in (1) prohibit closed-form expressions in the theoretical analysis. Therefore, we will also simplify the A2G channel to a deterministic LoS propagation model as a special case, in which all signals transmitted and received at the ABS will certainly experience the LoS propagation. This will improve the tractability in the system performance analysis.

2) G2G Channel: The G2G channels apply to the interference links between the interfering nodes and the UEs, e.g., from $\mathbf{z}_i$ to $\mathbf{u}_j$. Compared with the A2G channels, they are likely to be blocked at a much higher probability, for which the occurrence probabilities for the LoS and NLoS links are determined by [30]

$$\mathrm{P}_{\mathrm{GL}}(Z_{i,j}) = \begin{cases} 1 - \dfrac{Z_{i,j}}{d}, & \text{if } 0 < Z_{i,j} \leq d, \\ 0, & \text{if } Z_{i,j} > d, \end{cases} \qquad \mathrm{P}_{\mathrm{GN}}(Z_{i,j}) = 1 - \mathrm{P}_{\mathrm{GL}}(Z_{i,j}), \tag{3}$$

where d is a distance threshold depending on environments. By setting a smaller d, (3) depicts a scenario in which the ground terminals are surrounded by more obstacles. Moreover, (3) also shows that a UE is more likely to be interfered through the LoS propagation if the interfering node lies in a shorter distance $Z_{i,j}$.

Denoting by $\zeta_{\mathbf{z}_i,\mathbf{u}_j}$ the channel power gain from $\mathbf{z}_i$ to $\mathbf{u}_j$, we have

$$\zeta_{\mathbf{z}_i,\mathbf{u}_j} = Z_{i,j}^{-\alpha} g_{i,j,m}, \tag{4}$$

where $g_{i,j,m}$ is the small-scale channel power gain, and is identically and independently gamma distributed with fixed shape parameter $m \in \mathbb{N}^+$ and scale parameter $1/m$. Similar to the A2G channel, we set $\alpha = \alpha_{\mathrm{L}}$ and $\alpha = \alpha_{\mathrm{N}}$ for the LoS and NLoS propagations, and reduce m to 1 to yield Rayleigh fading for the NLoS propagation.

[1]Some correlation may exist between the A2G links, especially for the suburban and rural scenario. Hence, the independency assumption in this paper is more suitable for the dense urban scenario, where a lot of tall buildings may exist and they enrich the scatters around the ABSs.

C. Cooperative Transmission Scheme

Since no direct communication link is available from $\mathbf{b}$ to the UEs, the downlink transmission requires the assistance of ABSs in $\mathcal{R}$, which are working as relays. This implies that the users' data is delivered through a two-stage transmission protocol involving the wireless backhaul and the wireless access.[2] To be specific, in the first stage, $\mathbf{b}$ broadcasts the downlink data signals to all ABSs through wireless backhauls. After receiving the signals, each ABS will decode the data and check if it is correctly transmitted. According to the decoding results of the wireless backhauls, the ABSs will be divided into two groups, active ABSs that have successfully received the backhaul data, and idle ABSs that have failed to decode the backhaul data. In the second stage, the active ABSs will jointly forward the received signal to the UEs through wireless accesses. Above protocol is also referred to as selective decode-and-forward (DF) relaying scheme [31].[3]

To realize low-complexity cooperative communications, we assume that the active ABSs apply NC-JT to forward the signals in the wireless access. The NC-JT is most commonly adopted and easy to be implemented in cooperative systems. It takes the advantage of reduced overhead exchange among transmitters as a tight synchronization is not required. The basic idea of NC-JT is to make each transmitter directly transmit the same signals, of which only the phases are compensated. By carefully designing the cyclic delay length of each transmitters, a coherent power combination can be achieved at the receiver, yielding cyclic delay diversity and improving the signal-to-interference-plus-noise-ratio (SINR) from transmission [8], [18]. Mathematically, this coherent power combination is reflected as the sum of the channel power gains. Since the amplitude information of the channel is not utilized, this combination is evidently sub-optimal.

D. Downlink NOMA Transmission

We assume that the ABSs apply a power domain NOMA to simultaneously serve $\mathbf{u}_1$ and $\mathbf{u}_2$ on the same resource block. It is recognized that user detection ordering plays an important role in NOMA-based systems. A simple way is to order users according to their channel qualities, in which the performance gain of NOMA will diminish when these users statistically hold similar channel quality. Therefore, we consider another user pairing criterion in which users are ordered

[2]This dual-hop protocol can be extended to multi-hop relaying scenarios as presented in [22].

[3]We consider DF relaying instead of amplify-and-forward (AF) relaying. This is because, although AF relaying can reduce complexity at the ABSs, it will also bring in severe performance degradation for the NC-JT. Besides, by limiting the NOMA user number by 2 as recommended by 3GPP, the complexity will still be acceptable.

according to their quality of service (QoS) requirement. Specifically, assume that $\mathbf{u}_1$ demands higher priority to access the network but is with a lower transmission rate requirement R_1, such as IoT devices, while $\mathbf{u}_2$ can tolerate a longer delay but asks for a higher transmission rate R_2 ($R_2 > R_1$), such as file downloading users. Let s_j be the signal for $\mathbf{u}_j$. In the power domain NOMA, s_1 and s_2 are superimposed and the transmit power is divided according to the power allocation ratios β_1 and β_2. To guarantee the priority of $\mathbf{u}_1$ and a fixed total transmit power, we have $\beta_1 > \beta_2$ and $\beta_1 + \beta_2 = 1$. For simplicity, we use the same power allocation ratios for all wireless backhauls and wireless accesses.

The received signals at the ABSs and the UEs are composed by s_1 and s_2, and they will cause inter-user interference to each other. To mitigate the inter-user interference, we assume that successive interference cancellation (SIC) is employed at each receiver. According to the optimal decoding order of NOMA, s_1 should be decoded before s_2 at the receivers as shown in Fig. 1, because more power is allocated to s_1. Note that although we consider a two-user NOMA-based system for simplicity, which is recommended by 3GPP due to the complexity of SIC, our analysis framework can be easily extended to the case of more than two users.

E. Performance Metric and SINR Model

We take the outage probability as the key performance metric, which measures the occurrence probability of the event that the transmission rate is lower than the target rate. According to the Shannon formula, the target rates R_1 and R_2 can be translated to the target SINRs given by $\epsilon_1 = 2^{R_1} - 1$ and $\epsilon_2 = 2^{R_2} - 1$.

For the wireless backhauls, the SINRs $\gamma_{\mathbf{r}_k,1}$ and $\gamma_{\mathbf{r}_k,2}$ of s_1 and s_2 at $\mathbf{r}_k$ can be calculated as

$$\gamma_{\mathbf{r}_k,1} = \frac{\beta_1 P_{\mathbf{b}} \zeta_{\mathbf{b},\mathbf{r}_k}}{\sum_{\mathbf{z}_i \in \Phi} P_{\mathbf{z}} \zeta_{\mathbf{z}_i,\mathbf{r}_k} + \beta_2 P_{\mathbf{b}} \zeta_{\mathbf{b},\mathbf{r}_k} + \sigma^2} = \frac{\beta_1 W_{\mathbf{b},\mathbf{r}_k}}{I_{\mathbf{r}_k} + \beta_2 W_{\mathbf{b},\mathbf{r}_k} + 1}, \tag{5}$$

$$\gamma_{\mathbf{r}_k,2} = \frac{\beta_2 P_{\mathbf{b}} \zeta_{\mathbf{b},\mathbf{r}_k}}{\sum_{\mathbf{z}_i \in \Phi} P_{\mathbf{z}} \zeta_{\mathbf{z}_i,\mathbf{r}_k} + \sigma^2} = \frac{\beta_2 W_{\mathbf{b},\mathbf{r}_k}}{I_{\mathbf{r}_k} + 1}, \tag{6}$$

where $W_{\mathbf{b},\mathbf{r}_k} = \rho_{\mathbf{b}} \zeta_{\mathbf{b},\mathbf{r}_k}$ is the receive-side signal-to-noise-ratio (SNR) at $\mathbf{r}_k$, σ^2 is the power of additive white noise, $\rho_{\mathbf{b}} = P_{\mathbf{b}}/\sigma^2$ and $\rho_{\mathbf{z}} = P_{\mathbf{z}}/\sigma^2$ are transmit-side SNRs, and $I_{\mathbf{r}_k} = \sum_{\mathbf{z}_i \in \Phi} \rho_{\mathbf{z}} \zeta_{\mathbf{z}_i,\mathbf{r}_k}$ is the aggregate normalized interference from all interfering nodes to $\mathbf{r}_k$. It is revealed in (5) and (6) that, since s_1 is decoded before s_2 according to the decoding order of NOMA, s_2 will interfere with the decoding process of s_1. In contrast, interference caused by s_1 interfering with s_2 can be cancelled with the SIC if and only if s_1 is successfully decoded.

In our considered protocol, an ABS becomes active to provide wireless access if it successfully decodes both s_1 and s_2 in the wireless backhaul. Thus, the outage probability $\mathcal{O}_{\mathbf{r}_k}$ for $\mathbf{r}_k$ can be formally defined as

$$\mathcal{O}_{\mathbf{r}_k} = 1 - \mathbb{P}\left(\gamma_{\mathbf{r}_k,1} > \epsilon_1, \gamma_{\mathbf{r}_k,2} > \epsilon_2\right), \tag{7}$$

where $\mathbb{P}(\cdot)$ measures the occurrence probability of an event. For notation brevity, we set $p_k = 1 - \mathcal{O}_{\mathbf{r}_k}$, which also represents the active probability for $\mathbf{r}_k$ and stands for the reliability of the wireless backhaul.

For the wireless accesses, the SINRs $\gamma_{\mathbf{u}_1,1}$, $\gamma_{\mathbf{u}_2,1}$, and $\gamma_{\mathbf{u}_2,2}$ of s_1 at $\mathbf{u}_1$ and $\mathbf{u}_2$, and s_2 at $\mathbf{u}_2$ are calculated as

$$\gamma_{\mathbf{u}_1,1} = \frac{\beta_1 W_{\mathbf{r},\mathbf{u}_1}}{I_{\mathbf{u}_1} + \beta_2 W_{\mathbf{r},\mathbf{u}_1} + 1}, \tag{8}$$

$$\gamma_{\mathbf{u}_2,1} = \frac{\beta_1 W_{\mathbf{r},\mathbf{u}_2}}{I_{\mathbf{u}_2} + \beta_2 W_{\mathbf{r},\mathbf{u}_2} + 1}, \quad \text{and} \quad \gamma_{\mathbf{u}_2,2} = \frac{\beta_2 W_{\mathbf{r},\mathbf{u}_2}}{I_{\mathbf{u}_2} + 1}, \tag{9}$$

where $I_{\mathbf{u}_j} = \sum_{\mathbf{z}_i \in \Phi} \rho_{\mathbf{z}} \zeta_{\mathbf{z}_i,\mathbf{u}_j}$ is the aggregate normalized interference from all interfering nodes to $\mathbf{u}_j$, $W_{\mathbf{r},\mathbf{u}_j} = \sum_{k=1}^{K} W_{\mathbf{r}_k,\mathbf{u}_j} \mathbb{I}_k$ represents the sum of receive-side SNRs of all branches from all active ABSs, and $\mathbb{I}_k$ is an indicator equaling 1 if $\mathbf{r}_k$ is active and 0 otherwise. Because the active probability of $\mathbf{r}_k$ is p_k, we have $\mathbb{P}(\mathbb{I}_k = 1) = p_k$ and $\mathbb{P}(\mathbb{I}_k = 0) = 1 - p_k$. Note that the NC-JT relies on a carefully designed delay length instead of precoding to realize the combination of transmitted signals at the receivers, which is also referred to as cyclic delay diversity. Therefore, coherent power combinations in $W_{\mathbf{r},\mathbf{u}_1}$ and $W_{\mathbf{r},\mathbf{u}_2}$ are achievable for $\mathbf{u}_1$ and $\mathbf{u}_2$ simultaneously, which is hard for precoding based transmit diversity [32]. Rigorous derivations can be found in [8], [18]. Then, similar to (7), the outage probabilities $\mathcal{O}_{\mathbf{u}_1}$ and $\mathcal{O}_{\mathbf{u}_2}$ for $\mathbf{u}_1$ and $\mathbf{u}_2$ can be formally defined as

$$\mathcal{O}_{\mathbf{u}_1} = 1 - \mathbb{P}\left(\gamma_{\mathbf{u}_1,1} > \epsilon_1\right), \tag{10}$$

$$\mathcal{O}_{\mathbf{u}_2} = 1 - \mathbb{P}\left(\gamma_{\mathbf{u}_2,1} > \epsilon_1, \gamma_{\mathbf{u}_2,2} > \epsilon_2\right). \tag{11}$$

For clarity, we use $\hat{W}_{\mathbf{b},\mathbf{r}_k}$, $\hat{W}_{\mathbf{r}_k,\mathbf{u}_j}$, $\hat{W}_{\mathbf{r},\mathbf{u}_j}$, $\hat{I}_{\mathbf{r}_k}$, $\hat{p}_k$, and $\hat{\mathcal{O}}_{\mathbf{u}_j}$ to differentiate the notations under deterministic and probabilistic A2G models.

III. Distributions of the Receive-Side SNR

To obtain the outage probabilities, it is necessary to study the statistical characteristics of the SINRs, for which we start by analyzing the distributions of $W_{\mathbf{b},\mathbf{r}_k}$ and $W_{\mathbf{r},\mathbf{u}_j}$.

A. Receive-Side SNR Distribution for the Wireless Backhaul

According to $W_{\mathbf{b},\mathbf{r}_k} = \rho_{\mathbf{b}}\zeta_{\mathbf{b},\mathbf{r}_k}$ and (2), we can see that $W_{\mathbf{b},\mathbf{r}_k}$ follows gamma or exponential distributions according to the LoS conditions as

$$W_{\mathbf{b},\mathbf{r}_k} \overset{d}{\sim} \begin{cases} \mathrm{Exp}\left(\dfrac{1}{\vartheta_k}\right), & \text{if NLoS}, \\ \mathrm{Gamma}\left(\tilde{m}_k, \theta_k\right), & \text{if LoS}, \end{cases} \tag{12}$$

where $\mathrm{Exp}\left(\theta\right)$ is the exponential distribution with parameter θ, $\mathrm{Gamma}\left(m, \theta\right)$ is the gamma distribution with shape parameter m and scale parameter θ, $\vartheta_k = \rho_{\mathbf{b}}\tilde{D}_k^{-\alpha_{\mathrm{N}}}$, and $\theta_k = \rho_{\mathbf{b}}\tilde{D}_k^{-\alpha_{\mathrm{L}}}/\tilde{m}_k$. So the complementary cumulative distribution funcion (CCDF) of $W_{\mathbf{b},\mathbf{r}_k}$ is calculated as

$$\begin{aligned} \bar{F}_{W_{\mathbf{b},\mathbf{r}_k}}(w) &= \mathbb{P}\left(W_{\mathbf{b},\mathbf{r}_k} > w\right) \\ &= \mathrm{P}_{\mathrm{AN}}\left(\tilde{D}_k\right) \mathtt{ExpCCDF}\left(w, \frac{1}{\vartheta_k}\right) + \mathrm{P}_{\mathrm{AL}}\left(\tilde{D}_k\right) \mathtt{GamCCDF}\left(w, \tilde{m}_k, \theta_k\right), \end{aligned} \tag{13}$$

where $\mathtt{ExpCCDF}\left(w, \theta\right)$ is the CCDF of exponential distribution with parameter θ, and $\mathtt{GamCCDF}\left(w, m, \theta\right)$ is the CCDF of gamma distribution with shape parameter m and scale parameter θ.

B. Receive-Side SNR Distribution for the Wireless Access

We firstly provide the distribution of $W_{\mathbf{r}_k,\mathbf{u}_j}$, which is similar to $W_{\mathbf{b},\mathbf{r}_k}$

$$W_{\mathbf{r}_k,\mathbf{u}_j} \overset{d}{\sim} \begin{cases} \mathrm{Exp}\left(\dfrac{1}{\vartheta_{k,j}}\right), & \text{if NLoS}, \\ \mathrm{Gamma}\left(m_{k,j}, \theta_{k,j}\right), & \text{if LoS}, \end{cases} \tag{14}$$

where $\vartheta_{k,j} = \rho_{\mathbf{r}} D_{k,j}^{-\alpha_{\mathrm{N}}}$ and $\theta_{k,j} = \rho_{\mathbf{r}} D_{k,j}^{-\alpha_{\mathrm{L}}}/m_{k,j}$. Then, given that the wireless access is composed of the coherent combination of powers from different active ABSs, the cumulative distribution funciton (CDF) of $W_{\mathbf{r},\mathbf{u}_j}$ is provided in the following Lemma 1.

Lemma 1: Under the probabilistic LoS A2G propagation model, the CDF $F_{W_{\mathbf{r},\mathbf{u}_j}}(w)$ of the receive-side SNR $W_{\mathbf{r},\mathbf{u}_j}$ for the wireless access constituted by all links from active ABSs to $\mathbf{u}_j$ under the NC-JT and NOMA is given in (15), shown at the top of the next page, where $\mathtt{GamCDF}(w, \nu, \theta)$ is the CDF of gamma distribution with shape parameter ν and scale parameter θ, $Q = \prod_{k=1}^{K}(1-p_k)$, $\eta_{k,j,\nu}$, $\mu_{k,j,\nu}$, $\mathcal{Q}_{k,\nu}$, and $\mathcal{P}_{k,\nu}$ are given in (16), (17), (18), and (19), respectively, shown at the top of the next page, and $\binom{a}{b} = \frac{a!}{(a-b)!b!}$ denotes the binomial coefficient.[4]

[4]In (15), the summation over ν from 1 to a_k is naturally eliminated when $a_k = 0$.

$$F_{W_{\mathbf{r},\mathbf{r}_j}}(w) = Q\sum_{t_1=0}^{1}\cdots\sum_{t_K=0}^{1}\prod_{k=1}^{K}\left(\frac{p_k}{1-p_k}\right)^{t_k}\sum_{a_1=0}^{t_1}\cdots\sum_{a_K=0}^{t_K}\prod_{k=1}^{K}\mathrm{P}_{\mathrm{AN}}^{a_k}\left(D_{k,j}\right)\mathrm{P}_{\mathrm{AL}}^{t_k-a_k}\left(D_{k,j}\right)$$
$$\times\sum_{k=1}^{K}\left(\sum_{\nu=1}^{a_k}\frac{\eta_{k,j,\nu}}{\left(-\vartheta_{k,j}\right)^{-\nu}}\mathtt{GamCDF}\left(w,\nu,\vartheta_{k,j}\right)+\sum_{\nu=1}^{m_k(t_k-a_k)}\frac{\mu_{k,j,\nu}}{\left(-\theta_{k,j}\right)^{-\nu}}\mathtt{GamCDF}\left(w,\nu,\theta_{k,j}\right)\right). \quad (15)$$

$$\eta_{k,j,\nu} = \left(-\frac{1}{\vartheta_{k,j}}\right)^{a_k}\sum_{\mathcal{Q}_{k,\nu}}\prod_{n=1,n\neq k}^{K}\left(\binom{a_n+q_n-1}{q_n}\vartheta_{n,j}^{q_n}\left(1-\frac{\vartheta_{n,j}}{\vartheta_{k,j}}\right)^{-a_n-q_n}\right)$$
$$\times\prod_{n=1}^{K}\left(\binom{m_{n,j}(t_n-a_n)+p_n-1}{p_n}\theta_{n,j}^{p_n}\left(1-\frac{\theta_{n,j}}{\vartheta_{k,j}}\right)^{-m_{n,j}(t_n-a_n)-p_n}\right), \quad (16)$$

$$\mu_{k,j,\nu} = \left(-\frac{1}{\theta_{k,j}}\right)^{m_{k,j}(t_k-a_k)}\sum_{\mathcal{P}_{k,\nu}}\prod_{n=1}^{K}\left(\binom{a_n+q_n-1}{q_n}\vartheta_{n,j}^{q_n}\left(1-\frac{\vartheta_{n,j}}{\theta_{k,j}}\right)^{-a_n-q_n}\right)$$
$$\times\prod_{n=1,n\neq k}^{K}\left(\binom{m_{n,j}(t_n-a_n)+p_n-1}{p_n}\theta_{n,j}^{p_n}\left(1-\frac{\theta_{n,j}}{\theta_{k,j}}\right)^{-m_{n,j}(t_n-a_n)-p_n}\right), \quad (17)$$

$$\mathcal{Q}_{k,\nu}=\left\{(q_1,\cdots,q_K,p_1,\cdots,p_K)\Big|\sum_{n=1}^{K}q_n+\sum_{n=1}^{K}p_n=a_k-\nu,q_n\in\mathbb{N},p_n\in\mathbb{N},q_k=0\right\}, \quad (18)$$

$$\mathcal{P}_{k,\nu}=\left\{(q_1,\cdots,q_K,p_1,\cdots,p_K)\Big|\sum_{n=1}^{K}q_n+\sum_{n=1}^{K}p_n=m_{k,j}(t_k-a_k)-\nu,q_n\in\mathbb{N},p_n\in\mathbb{N},p_k=0\right\}. \quad (19)$$

If the A2G channel degrades to the deterministic LoS propagation model, then $F_{W_{\mathbf{r},\mathbf{u}_j}}(w)$ will be simplified as $F_{\hat{W}_{\mathbf{r},\mathbf{u}_j}}(w)$

$$F_{\hat{W}_{\mathbf{r},\mathbf{u}_j}}(w) = Q\sum_{t_1=0}^{1}\cdots\sum_{t_K=0}^{1}\prod_{k=1}^{K}\left(\frac{p_k}{1-p_k}\right)^{t_k}\sum_{k=1}^{K}\sum_{\nu=1}^{m_kt_k}\frac{\hat{\mu}_{k,j,\nu}}{\left(-\theta_{k,j}\right)^{-\nu}}\mathtt{GamCDF}(w,\nu,\theta_{k,j}), \quad (20)$$

where $\hat{\mu}_{k,j,\nu}$ and $\hat{\mathcal{P}}_{k,\nu}$ are given in (21) and (22), respectively, shown at the top of the next page.

Proof: See Appendix A. ■

IV. Downlink Performance Analysis

In this section, we study the downlink performance of the ABS-assisted system, including the active probability for the wireless backhauls, as well as the outage probability for the wireless

$$\hat{\mu}_{k,j,\nu} = \left(-\frac{1}{\theta_{k,j}}\right)^{m_{k,j}t_k} \sum_{\hat{\mathcal{P}}_{k,\nu}} \prod_{n=1,n\neq k}^{K} \left(\binom{m_{n,j}t_n + p_n - 1}{p_n} \frac{\theta_{n,j}^{p_n}}{\left(1-\frac{\theta_{n,j}}{\theta_{k,j}}\right)^{m_{n,j}t_n+p_n}} \right), \tag{21}$$

$$\hat{\mathcal{P}}_{k,\nu} = \left\{ (p_1, \cdots, p_K) | \sum_{n=1}^{K} p_n = m_{k,j}t_k - \nu, p_k = 0 \right\}. \tag{22}$$

accesses.

A. Active Probability for the Wireless Backhaul

The active probability of the ABS is defined by the occurrence probability of this ABS being able to successfully decode s_1 and s_2 simultaneously. It measures the reliability of the wireless backhaul from $\mathbf{b}$ to the ABS, and decides if this ABS can contribute to the wireless access. The following Theorem 1 provides the active probability p_k for $\mathbf{r}_k$.

Theorem 1: The active probability p_k for $\mathbf{r}_k$ is given by

$$\begin{aligned} p_k = {} & \mathrm{P}_{\mathrm{AN}}\left(\tilde{D}_k\right) \exp\left(-\frac{\xi_2}{\vartheta_k}\right) \mathcal{L}_{I_{\mathbf{r}_k}}\left(\frac{\xi_2}{\vartheta_k}\right) + \mathrm{P}_{\mathrm{AL}}\left(\tilde{D}_k\right) \exp\left(-\frac{\xi_2}{\theta_k}\right) \sum_{l=0}^{\tilde{m}_k-1} \left(\frac{\xi_2}{\theta_k}\right)^l \\ & \times \sum_{\kappa=0}^{l} \frac{(-1)^\kappa}{(l-\kappa)!} \sum_{(n_1,\cdots,n_\kappa)\in\mathcal{N}_\kappa} \frac{\mathcal{L}_{I_{\mathbf{r}_k}}\left(\frac{\xi_2}{\vartheta_k}\right)}{\prod_{\tau=1}^{\kappa}(n_\tau!)} \\ & \times \prod_{\tau=1}^{\kappa} \left(2\pi\lambda \int_h^\infty \left(\frac{\mathrm{P}_{\mathrm{AN}}(z)\left(-\rho_{\mathbf{z}} z^{-\alpha_{\mathrm{N}}}\right)^\tau}{\left(1+\frac{\xi_2\rho_{\mathbf{z}}}{\theta_k} z^{-\alpha_{\mathrm{N}}}\right)^{\tau+1}} + \binom{\tilde{m}-1+\tau}{\tilde{m}-1} \frac{\mathrm{P}_{\mathrm{AL}}(z)\left(-\frac{\rho_{\mathbf{z}}}{\tilde{m}} z^{-\alpha_{\mathrm{L}}}\right)^\tau}{\left(1+\frac{\xi_2\rho_{\mathbf{z}}}{\theta_k\tilde{m}} z^{-\alpha_{\mathrm{L}}}\right)^{\tau+\tilde{m}}} \right) z\mathrm{d}z \right)^{n_\tau}, \end{aligned} \tag{23}$$

where $\mathcal{N}_\kappa = \{(n_1, \cdots, n_\tau, \cdots, n_\kappa) | n_\tau \in \mathbb{N}, \sum_{\tau=1}^{\kappa} \tau \cdot n_\tau = \kappa\}$, $\xi_1 = \frac{\epsilon_1}{\beta_1 - \epsilon_1\beta_2}$, $\xi_2 = \max\left\{\xi_1, \frac{\epsilon_2}{\beta_2}\right\}$, and $\mathcal{L}_I(s) = \mathbb{E}_I\left[\mathrm{e}^{-sI}\right]$ is the Laplace transform (LT) of I given by

$$\mathcal{L}_{I_{\mathbf{r}_k}}(s) = \exp\left(-2\pi\lambda \int_h^\infty \left(1 - \frac{\mathrm{P}_{\mathrm{AN}}(z)}{1+s\rho_{\mathbf{z}} z^{-\alpha_{\mathrm{N}}}} - \frac{\mathrm{P}_{\mathrm{AL}}(z)}{\left(1+\frac{s\rho_{\mathbf{z}}}{\tilde{m}} z^{-\alpha_{\mathrm{L}}}\right)^{\tilde{m}}} \right) z\mathrm{d}z \right). \tag{24}$$

Proof: See Appendix B. ■

It is shown that the active probability in (23) involves an one-fold integral, which is due to the intractability in the occurrence probability of the LoS A2G propagation in (1). As a main feature of ABS assisted communications, the LoS propagation probability for the A2G link is much higher than that of the G2G link. Given this fact, we simplify the A2G channel model

to a deterministic LoS propagation model. This allows us to reach a closed-form expression for the active probability given in the following Corollary 1.

Corollary 1: Under the deterministic LoS A2G propagation model, the active probability $\hat{p}_k$ for $\mathbf{r}_k$ is given by

$$\hat{p}_k = \exp\left(-\frac{\xi_2}{\theta_k}\right) \sum_{l=0}^{\tilde{m}_k-1} \left(\frac{\xi_2}{\theta_k}\right)^l \sum_{\kappa=0}^{l} \binom{l}{\kappa} \frac{(-1)^\kappa}{l!} \mathcal{L}^{(\kappa)}_{\hat{I}_{\mathbf{r}_k}}\left(\frac{\xi_2}{\theta_k}\right). \tag{25}$$

The LT $\mathcal{L}_{\hat{I}_{\mathbf{r}_k}}(s)$ and its κ-th derivative $\mathcal{L}^{(\kappa)}_{\hat{I}_{\mathbf{r}_k}}(s)$ are respectively given in (26) and (27) as

$$\mathcal{L}_{\hat{I}_{\mathbf{r}_k}}(s) = \exp\left(-2\pi\lambda \sum_{n=1}^{\tilde{m}} \binom{\tilde{m}}{n} \left(\frac{s\rho_{\mathbf{z}}}{\tilde{m}}\right)^n \frac{h^{2-n\alpha_{\mathrm{L}}}}{n\alpha_{\mathrm{L}}-2} G\left(\tilde{m}, n-\frac{2}{\alpha_{\mathrm{L}}}, -\frac{1}{D_{\mathrm{H}}}\right)\right), \tag{26}$$

$$\begin{aligned}\mathcal{L}^{(\kappa)}_{\hat{I}_{\mathbf{r}_k}}(s) = \sum_{(n_1,\cdots,n_\kappa)\in\mathcal{N}_\kappa} \frac{\kappa!}{\prod_{\tau=1}^{\kappa}(n_\tau!)} \mathcal{L}_{\hat{I}_{\mathbf{r}_k}}(s) \prod_{\tau=1}^{\kappa} \Bigg(2\pi\lambda(-1)^\tau \binom{\tilde{m}-1+\tau}{\tilde{m}-1} \\ \times \left(\frac{\rho_{\mathbf{z}}}{\tilde{m}}\right)^\tau \frac{h^{2-\tau\alpha_{\mathrm{L}}}}{\tau\alpha_{\mathrm{L}}-2} G\left(\tilde{m}+\tau, \tau-\frac{2}{\alpha_{\mathrm{L}}}, -\frac{1}{D_{\mathrm{H}}}\right)\Bigg)^{n_\tau},\end{aligned} \tag{27}$$

where $G(a,b,c) = {}_2F_1(a,b;b+1,c)$ is the Gauss hypergeometric function [33] and can be efficiently computed by the build-in function "hypergeom" in MATLAB, and $D_{\mathrm{H}} = \frac{\tilde{m}}{s\rho_{\mathbf{z}}} h^{\alpha_{\mathrm{L}}}$.

Proof: The calculation of $\hat{p}_k$ in (25) directly follows the same way as $p_{k|\mathrm{L}}$ in (49) provided in Appendix B. Then $\mathcal{L}_{\hat{I}_{\mathbf{r}_k}}(s)$ is calculated as

$$\begin{aligned}\mathcal{L}_{\hat{I}_{\mathbf{r}_k}}(s) &= \mathbb{E}_\Phi\left[\prod_{\mathbf{z}_i\in\Phi} \mathbb{E}_{\tilde{Z}_{i,k}}\left[\frac{1}{\left(1+\frac{s\rho_{\mathbf{z}}}{\tilde{m}}\tilde{Z}_{i,k}^{-\alpha_{\mathrm{L}}}\right)^{\tilde{m}}}\right]\right] \\ &\overset{(g)}{=} \exp\left(-2\pi\lambda \int_h^\infty \frac{\sum_{n=1}^{\tilde{m}} \binom{\tilde{m}}{n} \left(\frac{s\rho_{\mathbf{z}}}{\tilde{m}}\right)^n z^{-n\alpha_{\mathrm{L}}}}{\left(1+\frac{s\rho_{\mathbf{z}}}{\tilde{m}} z^{-\alpha_{\mathrm{L}}}\right)^{\tilde{m}}} z\mathrm{d}z\right),\end{aligned} \tag{28}$$

where (g) is achieved by using the PGFL of PPP and binomial expansion. With the help of Gauss hypergeometric function, we can obtain the expression for $\mathcal{L}_{\hat{I}_{\mathbf{r}_k}}(s)$ provided in (26).

Finally, the expression for $\mathcal{L}^{(\kappa)}_{\hat{I}_{\mathbf{r}_k}}(s)$ can be calculated as in (27) by utilizing the Faà di Bruno formula [34]. The detail of the derivation is omitted due to space limit. ■

B. Outage Probability for the Wireless Access

With p_k and the CDF of $W_{\mathbf{r},\mathbf{u}_j}$, the outage probability for $\mathbf{u}_j$ can be easily derived, and is provided in the following Theorem 2.

$$\mathcal{O}_{\mathbf{u}_j} = Q \sum_{t_1=0}^{1} \cdots \sum_{t_K=0}^{1} \prod_{k=1}^{K} \left(\frac{p_k}{1-p_k}\right)^{t_k} \sum_{a_1=0}^{t_1} \cdots \sum_{a_K=0}^{t_K} \prod_{k=1}^{K} \mathrm{P}_{\mathrm{AN}}^{a_k}\left(D_{k,j}\right) \mathrm{P}_{\mathrm{AL}}^{t_k-a_k}\left(D_{k,j}\right)$$
$$\times \sum_{k=1}^{K} \left(\sum_{\nu=1}^{a_k} \frac{\eta_{k,j,\nu}}{(-\vartheta_{k,j})^{-\nu}} \left(1 - \exp\left(-\frac{\xi_j}{\vartheta_{k,j}}\right) \sum_{l=0}^{\nu-1} \left(\frac{\xi_j}{\vartheta_{k,j}}\right)^l \sum_{\kappa=0}^{l} \binom{l}{\kappa} \frac{(-1)^\kappa}{l!} \mathcal{L}_{I_{\mathbf{u}_j}}^{(\kappa)}\left(\frac{\xi_j}{\vartheta_{k,j}}\right)\right) \right.$$
$$\left. + \sum_{\nu=1}^{m_{k,j}(t_k-a_k)} \frac{\mu_{k,j,\nu}}{(-\theta_{k,j})^{-\nu}} \left(1 - \exp\left(-\frac{\xi_j}{\theta_{k,j}}\right) \sum_{l=0}^{\nu-1} \left(\frac{\xi_j}{\theta_{k,j}}\right)^l \sum_{\kappa=0}^{l} \binom{l}{\kappa} \frac{(-1)^\kappa}{l!} \mathcal{L}_{I_{\mathbf{u}_j}}^{(\kappa)}\left(\frac{\xi_j}{\theta_{k,j}}\right)\right)\right). \quad (29)$$

$$\mathcal{L}_{I_{\mathbf{u}_j}}(s) = \exp\left(-2\pi\lambda\frac{d^2}{3} G\left(1, \frac{3}{\alpha_{\mathrm{N}}}, -D_{\mathrm{N}}\right) - 2\pi\lambda \frac{s\rho_{\mathbf{z}} d^{2-\alpha_{\mathrm{N}}}}{\alpha_{\mathrm{N}}-2} G\left(1, 1-\frac{2}{\alpha_{\mathrm{N}}}, -\frac{1}{D_{\mathrm{N}}}\right)\right)$$
$$\times \exp\left(-2\pi\lambda \sum_{n=1}^{m} \binom{m}{n} \left(\frac{m}{s\rho_{\mathbf{z}}}\right)^{m-n} d^{(m-n)\alpha_{\mathrm{L}}+2}\right.$$
$$\left. \times \left(\frac{G\left(m, m-n+\frac{2}{\alpha_{\mathrm{L}}}, -D_{\mathrm{L}}\right)}{(m-n)\alpha_{\mathrm{L}}+2} - \frac{G\left(m, m-n+\frac{3}{\alpha_{\mathrm{L}}}, -D_{\mathrm{L}}\right)}{(m-n)\alpha_{\mathrm{L}}+3}\right)\right), \quad (30)$$

$$\mathcal{L}_{I_{\mathbf{u}_j}}^{(\kappa)}(s) = \sum_{(n_1,\cdots,n_\kappa)\in\mathcal{N}_\kappa} \frac{\kappa!}{\prod_{\tau=1}^{\kappa}(n_\tau!)} \mathcal{L}_{I_{\mathbf{u}_j}}(s) \prod_{\tau=1}^{\kappa} \left(2\pi\lambda(-1)^\tau \left(\frac{d^{2+\alpha_{\mathrm{N}}}\rho_{\mathbf{z}}^{-1}}{(3+\alpha_{\mathrm{N}})s^{\tau+1}} G\left(\tau+1, \frac{3}{\alpha_{\mathrm{N}}}+1, -D_{\mathrm{N}}\right)\right.\right.$$
$$+ \frac{\rho_{\mathbf{z}}^{\tau} d^{2-\tau\alpha_{\mathrm{N}}}}{\tau\alpha_{\mathrm{N}}-2} G\left(\tau+1, \tau-\frac{2}{\alpha_{\mathrm{N}}}, -\frac{1}{D_{\mathrm{N}}}\right) + \binom{m-1+\tau}{m-1}\left(\frac{m}{\rho_{\mathbf{z}}}\right)^m$$
$$\left.\left. \times \frac{d^{m\alpha_{\mathrm{L}}+2}}{s^{\tau+m}} \left(\frac{G\left(m+\tau, m+\frac{2}{\alpha_{\mathrm{L}}}, -D_{\mathrm{L}}\right)}{m\alpha_{\mathrm{L}}+2} - \frac{G\left(m+\tau, m+\frac{3}{\alpha_{\mathrm{L}}}, -D_{\mathrm{L}}\right)}{m\alpha_{\mathrm{L}}+3}\right)\right)\right)^{n_\tau}. \quad (31)$$

Theorem 2: The outage probability $\mathcal{O}_{\mathbf{u}_j}$ for $\mathbf{u}_j$ is given in (29), shown at the top of this page, where the LT $\mathcal{L}_{I_{\mathbf{u}_j}}(s)$ of $I_{\mathbf{u}_j}$ and its κ-th derivative $\mathcal{L}_{I_{\mathbf{u}_j}}^{(\kappa)}(s)$ are respectively given in (30) and (31), also shown at the top of this page, $D_{\mathrm{N}} = \frac{d^{\alpha_{\mathrm{N}}}}{s\rho_{\mathbf{z}}}$, and $D_{\mathrm{L}} = \frac{m}{s\rho_{\mathbf{z}}} d^{\alpha_{\mathrm{L}}}$.

Proof: Similar to Theorem 1, the derivation can be readily conducted for the general J-user case, so that we will mainly focus on the 2-user case. By defining $\xi_1 = \frac{\epsilon_1}{\beta_1 - \epsilon_1\beta_2}$ and $\xi_2 = \max\left\{\xi_1, \frac{\epsilon_2}{\beta_2}\right\}$, we can express $\mathcal{O}_{\mathbf{u}_1}$ and $\mathcal{O}_{\mathbf{u}_2}$ with one unified expression as $\mathcal{O}_{\mathbf{u}_j} = \mathbb{P}\left(W_{\mathbf{r},\mathbf{u}_j} < \xi_j\left(I_{\mathbf{u}_j}+1\right)\right)$. Then by setting $w = \xi_j\left(I_{\mathbf{u}_j}+1\right)$ and using (15), we can reach the expression for $\mathcal{O}_{\mathbf{u}_j}$ provided in (29), involving the κ-th derivative of the LT of $I_{\mathbf{u}_j}$. Noting that

the ground interfering nodes can be any close to $\mathbf{u}_j$, we can calculate $\mathcal{L}_{I_{\mathrm{u}_j}}(s)$ as

$$\mathcal{L}_{I_{\mathrm{u}_j}}(s) = \mathbb{E}\left[\exp\left(-s\sum_{\mathbf{z}_i\in\Phi}\rho_{\mathbf{z}}\zeta_{\mathbf{z}_i,\mathbf{u}_j}\right)\right] = \mathbb{E}_{\Phi}\left[\prod_{\mathbf{z}_i\in\Phi}\mathbb{E}_{\zeta_{\mathbf{z}_i,\mathbf{u}_j}}\left[\exp\left(-s\rho_{\mathbf{z}}\zeta_{\mathbf{z}_i,\mathbf{u}_j}\right)\right]\right]$$
$$\overset{(h)}{=} \mathbb{E}_{\Phi}\left[\prod_{\mathbf{z}_i\in\Phi}\mathbb{E}_{Z_{i,j},g_{i,j,m}}\left[\mathrm{P}_{\mathrm{GN}}\left(Z_{i,j}\right)\exp\left(-s\rho_{\mathbf{z}}Z_{i,j}^{-\alpha_{\mathrm{N}}}g_{i,j,1}\right)+\mathrm{P}_{\mathrm{GL}}\left(Z_{i,j}\right)\exp\left(-s\rho_{\mathbf{z}}Z_{i,j}^{-\alpha_{\mathrm{L}}}g_{i,j,m}\right)\right]\right]$$
$$\overset{(i)}{=} \exp\left(-2\pi\lambda\left(\int_0^d\left(1-\frac{z}{d}\frac{1}{1+s\rho_{\mathbf{z}}z^{-\alpha_{\mathrm{N}}}}-\left(1-\frac{z}{d}\right)\frac{1}{\left(1+\frac{s\rho_{\mathbf{z}}}{m}z^{-\alpha_{\mathrm{L}}}\right)^m}\right)z\mathrm{d}z\right.\right.$$
$$\left.\left.+\int_d^{\infty}\left(1-\frac{1}{1+s\rho_{\mathbf{z}}z^{-\alpha_{\mathrm{N}}}}\right)z\mathrm{d}z\right)\right), \tag{32}$$

where (h) follows from the probabilistic LoS and NLoS G2G interference propagation, and (i) is obtained by utilizing the PGFL of the PPP and (3). With the help again of Gauss hypergeometric function, we can achieve the expression for $\mathcal{L}_{I_{\mathrm{u}_j}}(s)$ provided in (30).

Finally, by applying the Faà di Bruno formula, we can evaluate $\mathcal{L}^{(\kappa)}_{I_{\mathbf{u}_j}}(s)$ provided in (31). ■

Under the deterministic LoS A2G channel model, the outage probability $\mathcal{O}_{\mathbf{u}_j}$ will be simplified as $\hat{\mathcal{O}}_{\mathbf{u}_j}$ and is provided in the following Corollary 2.

Corollary 2: The outage probability $\hat{\mathcal{O}}_{\mathbf{u}_j}$ for $\mathbf{u}_j$ under the deterministic LoS A2G channel model is given by

$$\hat{\mathcal{O}}_{\mathbf{u}_j} = Q\sum_{t_1=0}^{1}\cdots\sum_{t_K=0}^{1}\prod_{k=1}^{K}\left(\frac{p_k}{1-p_k}\right)^{t_k}\sum_{k=1}^{K}\sum_{\nu=1}^{m_{k,j}t_k}\frac{\hat{\mu}_{k,j,\nu}}{(-\theta_{k,j})^{-\nu}}$$
$$\times\left(1-\exp\left(-\frac{\xi_j}{\theta_{k,j}}\right)\sum_{l=0}^{\nu-1}\left(\frac{\xi_j}{\theta_{k,j}}\right)^l\sum_{\kappa=0}^{l}\binom{l}{\kappa}\frac{(-1)^{\kappa}}{l!}\mathcal{L}^{(\kappa)}_{I_{\mathbf{u}_j}}\left(\frac{\xi_j}{\theta_{k,j}}\right)\right), \tag{33}$$

where $\hat{\mu}_{k,j,\nu}$ and $\mathcal{L}^{(\kappa)}_{I_{\mathbf{u}_j}}(s)$ are given in (21) and (31).

Proof: The proof follows a similar procedure as the proof of Theorem 2. ■

It can be seen that $\hat{\mathcal{O}}_{\mathbf{u}_j}$ and $\mathcal{O}_{\mathbf{u}_j}$ share the same $\mathcal{L}^{(\kappa)}_{I_{\mathbf{u}_j}}(s)$. This is because switching the probabilistic LoS A2G channel to the deterministic one will not influence interference from $\mathbf{z}_i$ to $\mathbf{u}_j$. Although (33) is presented in a closed-form, the expression is still complicated to analyze the outage performance. Thus, we further provide the outage probability expression in the high transmit SNR region in the following Corollary 3 to study the impact of the unreliable wireless backhauls.

Corollary 3: In the high ABS transmit SNR region, i.e., $\rho_{\mathbf{r}} \to \infty$, if the transmit power of the interfering nodes is fixed, then the outage probability $\check{\mathcal{O}}_{\mathbf{u}_j}$ for $\mathbf{u}_j$ can be calculated by $\check{\mathcal{O}}_{\mathbf{u}_j} = \prod_{k=1}^{K}(1-p_k)$.

Proof: By the definition of the Gauss hypergeometry function, it can be proved that when $s \to 0$, we will have $\mathcal{L}_{I_{\mathbf{u}_j}}(s) \to 1$, $s^l \cdot \mathcal{L}^{(\kappa)}_{I_{\mathbf{u}_j}}(s) \to 1$ for $l = 0$, and $s^l \cdot \mathcal{L}^{(\kappa)}_{I_{\mathbf{u}_j}}(s) \to 0$ for $l > 0$. Thus, finally we can obtain the expression for $\check{\mathcal{O}}_{\mathbf{u}_j}$. ■

Corollary 3 shows a floor for the outage probability, which will be discussed in Section V.

C. Comparison with the Orthogonal Multiple Access-Based Transmission

We finally compare the outage probability of the NOMA system with that of the OMA system, e.g., time division multiple access (TDMA). In TDMA, to avoid interference between each other, $\mathbf{u}_1$ and $\mathbf{u}_2$ should take turns to be served. Given the same spectrum bandwidth, such transmission requires twice as many time resources as NOMA. Hence, in the serving duration of each UE in the OMA system, the transmission should support twice as high as the rate targeted by the NOMA system. Under the above OMA protocol, the conditions provided in the following Corollary 4 will suffice to summarize the advantage of NOMA over OMA in the aspect of outage probability.

Corollary 4: The NOMA transmission will guarantee higher reliability for the wireless backhaul than the OMA transmission if $\frac{1}{2^{R_2}+1} < \beta_2 < \frac{2^{2R_2-R_1}-1}{2^{2R_2}-1}$ is satisfied. Meanwhile, for the wireless access, a lower outage probability can be expected under the NOMA transmission for $\mathbf{u}_1$ if $\beta_2 < \frac{1}{2^{R_1}+1}$ is satisfied, and for $\mathbf{u}_2$ if $\frac{1}{2^{R_2}+1} < \beta_2 < \frac{2^{2R_2-R_1}-1}{2^{2R_2}-1}$ is satisfied.

Proof: With the additive noise omitted, the reliability of the wireless backhaul for NOMA and OMA are respectively given by

$$p_k^{\mathrm{NOMA}} = \mathbb{P}\left(\frac{W_{\mathbf{b},\mathbf{r}_k}}{I_{\mathbf{r}_k}} > \frac{2^{R_1}-1}{1-2^{R_1}\beta_2}, \frac{W_{\mathbf{b},\mathbf{r}_k}}{I_{\mathbf{r}_k}} > \frac{2^{R_2}-1}{\beta_2}\right),$$
$$p_k^{\mathrm{OMA}} = \mathbb{P}\left(\frac{W_{\mathbf{b},\mathbf{r}_k}}{I_{\mathbf{r}_k}} > 2^{2R_2}-1\right). \tag{34}$$

Hence, a lower outage probability can be guaranteed for NOMA if $\frac{2^{R_1}-1}{1-2^{R_1}\beta_2} < 2^{2R_2}-1$ and $\frac{2^{R_2}-1}{\beta_2} < 2^{2R_2}-1$ are satisfied at the same time. This requires $\frac{1}{2^{R_2}+1} < \beta_2 < \frac{2^{2R_2-R_1}-1}{2^{2R_2}-1}$. As for the wireless access, the derivation follows a similar way and is hence omitted. ■

Above Corollary 4 provides instructions on how to properly select the NOMA power allocation coefficient, and will be further discussed in Section V.

V. Numerical Results and Discussions

In this section, we firstly compare the outage probability results with the Monte Carlo simulation-based results to verify the accuracy of the analytical expressions. Then, we study the impacts

of main system parameters including the reliability of the wireless backhaul, ABS number, and target transmission rate on the performance metrics. Finally, we also compare the system performance of the NOMA-based transmission with the basic OMA-based transmission.

We consider a dense urban environment, for which the environment parameters to determine LoS and NLoS propagation are set to be $b = 0.136$, $c = 11.95$ as in [12] for the A2G channel, and $d = 400$ m as in [30] for the G2G channel. The power of the additive white noise is $\sigma^2 = -90$ dBm. The system performance is investigated under two location sets, i.e., S_1 and S_2, in Cartesian coordinates both including $K = 4$ ABSs. In specific, we have $\mathcal{R} = \{(50, 0), (0, 100), (-150, 0), (0, -200)\}$ for S_1 and $\mathcal{R} = \{(50, 50), (-50, 25), (0, -50), (50, -50)\}$ for S_2, while the locations of the UEs are fixed at $\mathbf{u}_1 = \left(-50, -50\sqrt{3}\right)$ and $\mathbf{u}_2 = (-50, 0)$. Unless otherwise stated, the height of the ABSs is $h = 50$ m, the NOMA power allocation coefficient for $\mathbf{u}_1$ is $\beta_1 = 0.7$, the path-loss exponents are $\alpha_{\mathrm{L}} = 2.8$ and $\alpha_{\mathrm{N}} = 3.8$ for LoS and NLoS links, respectively, the Nakagami-m parameters are $\tilde{m} = 4$, $m = 3$, and $m_{k,j} = \{4, 4, 2, 2; 4, 4, 2, 2\}$,[5] and the interfering node density is $\lambda = \frac{1}{500^2\pi}$ per square meter.

A. *Validation of Results*

We firstly validate our analytical expressions for the outage probability under different interfering node densities (i.e., $\lambda = \frac{1}{500^2\pi}$ and $\frac{1}{250^2\pi}$ nodes per square meter, respectively) in Fig. 3a and Fig. 3b. The analytical results are examined by comparing with link-level simulation results, which are averaged over 100000 independent runs. The simulations are performed in a large circular area with a radius of 25 km. The accuracy investigations are performed under location sets S_1 and S_2, respectively, where probabilistic LoS A2G channel is applied for S_1 with $\tilde{m}_k = \{4, 4, 2, 2\}$ and deterministic LoS A2G channel is applied for S_2 with $\tilde{m}_k = \{3, 3, 2, 2\}$. The target rate of $\mathbf{u}_1$ is fixed as $R_1 = 1$ bps/Hz.

Fig. 3a plots the outage probabilities $\mathcal{O}_{\mathbf{u}_1}$ and $\mathcal{O}_{\mathbf{u}_2}$ with the target rate R_2, while Fig. 3b plots the same performance metric with the transmit power $P_{\mathbf{s}}$ of the MBS. Both figures show that the derived outage probability results perfectly match the simulation results for both probabilistic and deterministic LoS A2G channels. This confirms that our following studies on the impacts of other system parameters and the superiority of NOMA are valid. Another observation in Fig. 3a is that, with the increase of R_2, $\mathcal{O}_{\mathbf{u}_1}$ will also deteriorate, although R_1 is fixed for $\mathbf{u}_1$. This is

[5] According to [35] and some modifications, we only consider $m \leq 4$ in the simulations.

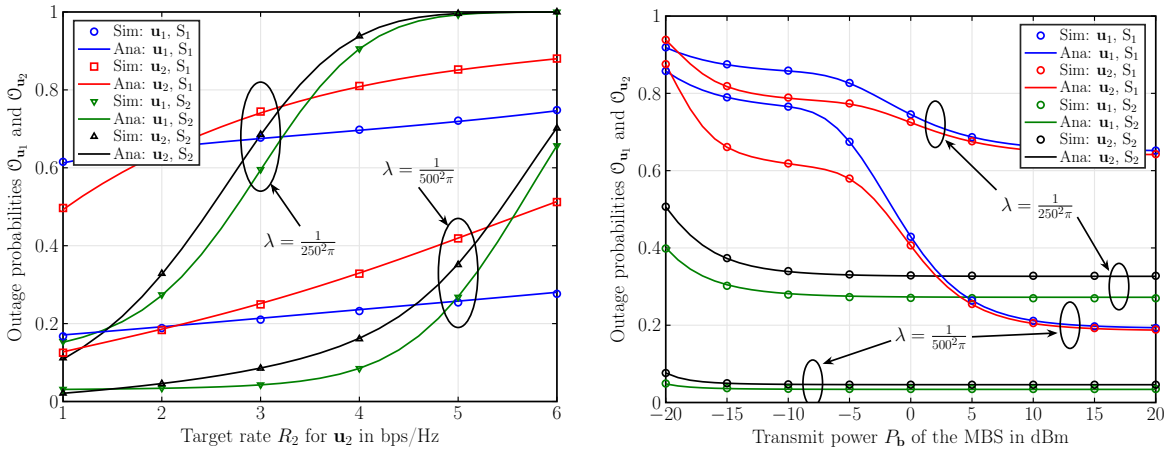

(a) Accuracy investigation against varying target rate R_2 with $P_{\mathbf{b}} = 40$ dBm and $P_{\mathbf{r}} = P_{\mathbf{z}} = 37$ dBm.

(b) Accuracy investigation against varying transmit power $P_{\mathbf{b}}$ with $P_{\mathbf{r}} = P_{\mathbf{z}} = P_{\mathbf{b}}/2$ and target rate $R_2 = 2$ bps/Hz.

Fig. 3. Outage probabilities $\mathcal{O}_{\mathbf{u}_1}$ and $\mathcal{O}_{\mathbf{u}_2}$ vs. target rate R_2 and transmit power $P_{\mathbf{b}}$ of the MBS under various interfering node density λ with $R_1 = 1$ bps/Hz. Probabilistic LoS A2G channel is applied for S_1 with $\tilde{m}_k = \{4, 4, 2, 2\}$, while deterministic LoS A2G chanel is applied for S_2 with $\tilde{m}_k = \{3, 3, 2, 2\}$.

because the data transmission of $\mathbf{u}_1$ also relies on the relaying function of $\mathbf{r}_k$, which will be active only if the data for $\mathbf{u}_1$ and $\mathbf{u}_2$ are both successfully decoded in the wireless backhaul. In Fig. 3b, it is shown that the outage probaiblity will decrease with the increase of the transmit power $P_{\mathbf{b}}$ and $P_{\mathbf{r}}$. However, an outage probability floor can be observed for all cases. Because the transmit power $P_{\mathbf{z}}$ is set to be proportional to $P_{\mathbf{b}}$ and $P_{\mathbf{r}}$. With the increase of transmit power, the system will become interference limited instead of noise limited, for which transmitting with more power will not bring in any improvement in the outage performance. Fig. 3b also presents another floor caused by the wireless backhaul for location set S_1, which will be investigated in Fig. 4 later. Besides, an outage probability increment can be observed in both figures for the denser interfering nodes scenario, which is in line with intuition.

B. Impacts of System Parameters

Based on the derived analytical expressions, we will now study the impacts of various parameters including the wireless backhaul reliability, ABS number, and target transmission rate on the performance metrics.

1) Impacts of Backhaul Reliability and ABS Number: In Fig. 4a and Fig. 4b, we investigate the impact of the reliability of wireless backhaul. To this end, we fix the active probability of

each ABS at different level $p_k = \bar{p}$ to study the system outage probability and outage sum rate for various target rates for $\mathbf{u}_2$ (i.e., $R_2 = 2$ bps/Hz and 4 bps/Hz). The results are obtained under location set S_1 and the target rate for $\mathbf{u}_1$ is fixed at $R_1 = 1$ bps/Hz. We also fix the power of the interfering nodes as $P_{\mathbf{z}} = -20$ dBm, hence the system stays in the noise-limited region.

Fig. 4a plots the system outage probability $\mathcal{O}_{\mathrm{NOMA}}$, which is defined as the probability that $\mathbf{u}_1$ or $\mathbf{u}_2$ is not able to successfully decode its signal. The results show that an outage probability floor exists with the increase of $P_{\mathbf{r}}$ for all cases under a specific backhaul reliability. According to Corollary 3, this floor is determined by the value of $\bar{p}$ instead of R_2 or the A2G channel model. This is because the success transmission probaiblity of the wireless access will approach one with the increase of $P_{\mathbf{r}}$ in a noise-limited system, therefore the overall outage performance is constrained by the wireless backhaul. Besides, in low transmit SNR region, the system can expect a better outage performance under the deterministic LoS A2G channel due to the benefit of LoS link signal transmission.

Fig. 4b shows similar performance floors due to the constraint of wireless backhaul by plotting the outage sum rate of the system, which is by definition calculated as $R_1\left(1-\mathcal{O}_{\mathbf{u}_1}\right)+R_2\left(1-\mathcal{O}_{\mathbf{u}_2}\right)$. It shows that $\bar{p}$ is one of the decisive parameters for the outage sum rate. The target rate R_2 is also playing a dominant role, which is fairly self-explanatory through the definition of the outage sum rate.

In Fig. 4b, we also study the improvement brought in by deploying more ABSs. For two investigated active probability (i.e., $\bar{p} = 0.8$ and 0.9), we obtain the results by choosing the first K coordinates in location set S_1 and first K columns in $m_{k,j}$. The results show that, under the same target rate R_2, a higher outage sum rate is achievable when more ABSs are deployed. The reason is two-fold. On one hand, more ABSs increase the diversity for the wireless access, because the transmit power of each active ABS can be coherently combined at both $\mathbf{u}_1$ and $\mathbf{u}_2$ concurrently, with the cyclic delay based NC-JT. On the other hand, adding ABSs can improve the reliability for the overall wireless backhaul, which determines the outage probability floor as discussed previously. As the evident, the performance gap between $\bar{p} = 0.9$ and 0.8 shown in Fig.4b is much smaller when more ABSs are deployed. This indicates that the constraint of unreliable wireless backhaul can be compensated by increasing the number of ABSs.

2) Impacts of ABS Height and A2G Channel Model: In Fig. 5a, we plot the system outage probability $\mathcal{O}_{\mathrm{NOMA}}$ with ABS height h under probabilistic and deterministic LoS A2G channel. The results are obtained under location set S_1 with $\tilde{m}_k = \{4, 4, 2, 2\}$, the target rates are $R_1 =$

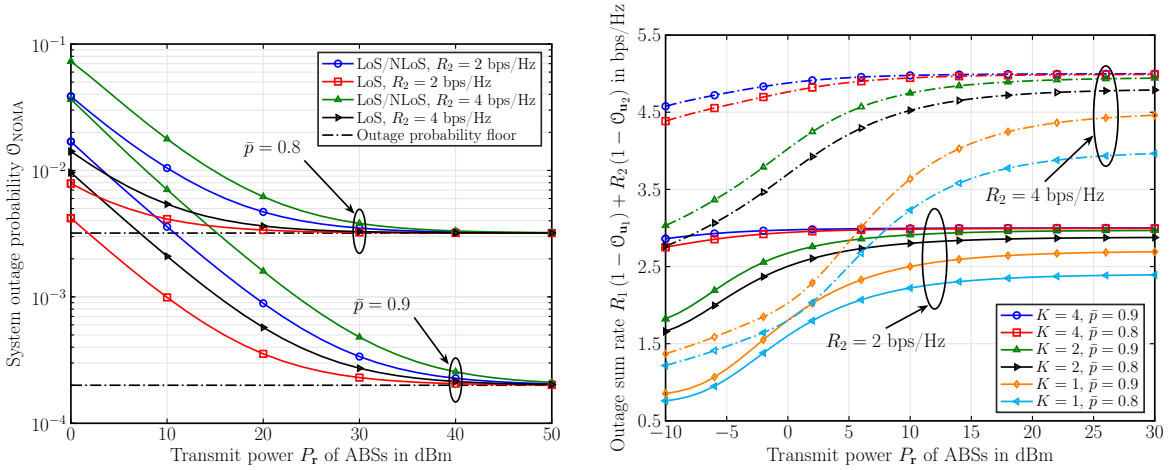

(a) Impacts of backhaul reliability.

(b) Impacts of backhaul reliability and ABS number.

Fig. 4. System outage probability $\mathcal{O}_{\text{NOMA}}$ and outage sum rate $R_1(1-\mathcal{O}_{\mathbf{u}_1}) + R_2(1-\mathcal{O}_{\mathbf{u}_2})$ vs. transmit power $P_{\mathbf{r}}$ of ABSs under various values of active probability p_k and target rate R_2, with $P_{\mathbf{z}} = -20$ dBm, location set S_1, and $R_1 = 1$ bps/Hz.

1 bps/Hz and $R_2 = 2$ bps/Hz, and the transmit powers are $P_{\mathbf{b}} = 40$ dBm and $P_{\mathbf{r}} = P_{\mathbf{z}} = 37$ dBm.

It is observed that, an optimal height exists for each curve under probabilistic LoS A2G channel to obtain the lowest $\mathcal{O}_{\text{NOMA}}$. On the contrary, $\mathcal{O}_{\text{NOMA}}$ will monotonically increase with h under deterministic LoS A2G channel. Recall that, with (1), the signal transmission will be more likely to experience LoS propagation at a higher altitude under the probabilistic model. So transmissions from the sky result in a positive impact on the outage probability. However, as h increases, the transmission distance is stretched, so that an additional attenuation can be observed from the transmitted signal. Therefore, the two counteracting impacts will be balanced and lead to an optimal height. As for the deterministic LoS A2G channel, increasing h will only bring in a negative impact on the system performance. This is because the propagation condition of the A2G transmitted signal is not related to h and will certainly experience LoS propagation.

3) Impacts of Nakagami-m Parameter and Rate Requirement: Fig. 5b plots the system outage probability $\mathcal{O}_{\text{NOMA}}$ with target rate R_1 for $\mathbf{u}_1$ for various indentical Nakagami-m parameters, (i.e., the Nakagami-m parameters for different links equal the same $\bar{m}$) and R_2/R_1 ratios. The location set is S_1 under probabilistic LoS A2G channel, and the transmit powers are fixed at $P_{\mathbf{b}} = P_{\mathbf{r}} = 20$ dBm and $P_{\mathbf{z}} = 0$ dBm.

The results in Fig. 5b show that $\mathcal{O}_{\text{NOMA}}$ will increase with $\bar{m}$. This is in line with the property of Nakagami-m fading that a larger m represents a better gathering effect of the

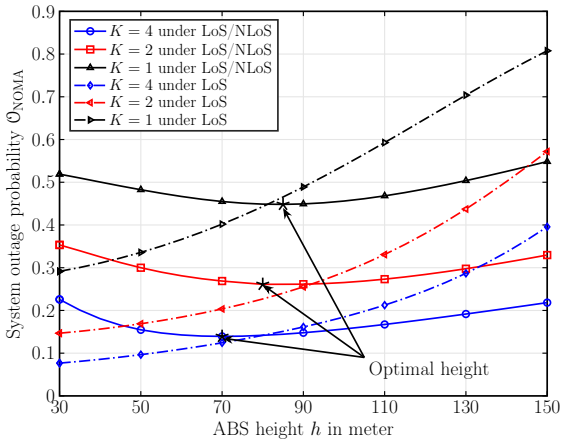

(a) Impacts of ABS height with $P_{\mathbf{b}} = 40$ dBm, $P_{\mathbf{r}} = P_{\mathbf{z}} = 37$ dBm, $R_2 = 2R_1 = 2$ bps/Hz, and $\tilde{m}_k = \{4, 4, 2, 2\}$.

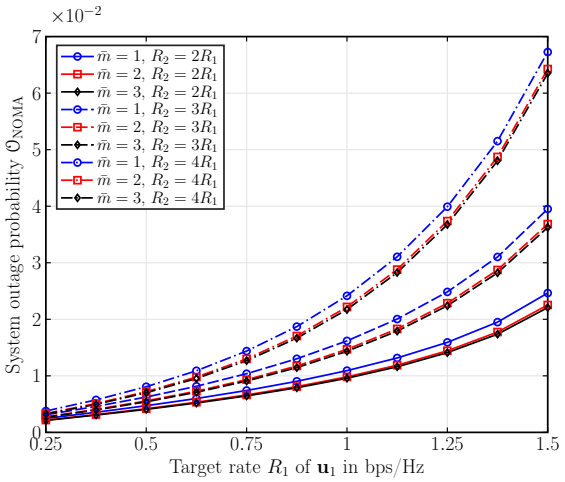

(b) Impacts of target rate R_1 with $P_{\mathbf{b}} = P_{\mathbf{r}} = 20$ dBm, $P_{\mathbf{z}} = 0$ dBm under probabilistic LoS A2G channel.

Fig. 5. System outage probability $\mathcal{O}_{\text{NOMA}}$ vs. ABS height h and target rate R_1 of $\mathbf{u}_1$ under various values of ABS number K, Nakagami-m parameter, and R_2/R_1 ratio, with location set S_1.

propagation. Nevertheless, the performance gap is not obvious, especially when $\bar{m}$ is given a larger value. Moreover, the results also show that the system outage probability increases as the rate requirement of either $\mathbf{u}_1$ or $\mathbf{u}_2$ increases.

C. Comparison with OMA Transmission

We finally compare the NOMA and OMA transmissions from the aspects of backhaul reliability, outage probability, outage sum rate, and energy efficiency in Fig. 6 and Fig. 7.

Fig. 6a and Fig. 6b plot the backhaul reliability and outage probability with NOMA power allocation coefficient β_2 under NOMA and OMA transmissions. The location set is S_1 with $\tilde{m}_k = \{4, 4, 2, 2\}$ under probabilistic LoS A2G channel, the transmit power of the interfering nodes is $P_{\mathbf{z}} = 37$ dBm, and the target rate is $R_1 = 1$ bps/Hz. Since OMA involves in no power partitioning among UEs, the results of the OMA case remain unchanged with β_2.

Fig. 6a firstly compares the backhaul reliability p_k of NOMA with that of OMA under $P_{\mathbf{b}} = 40$ dBm. The results show that NOMA can bring in a more reliable wireless backhaul than OMA. But this superiority closely depends on the value of the NOMA power allocation coefficient β_2. To achieve higher backhaul reliability, β_2 should satisfy $\frac{1}{2^{2R_2}+1} < \beta_2 < \frac{2^{2R_2-R_1}-1}{2^{2R_2}-1}$, which suggests

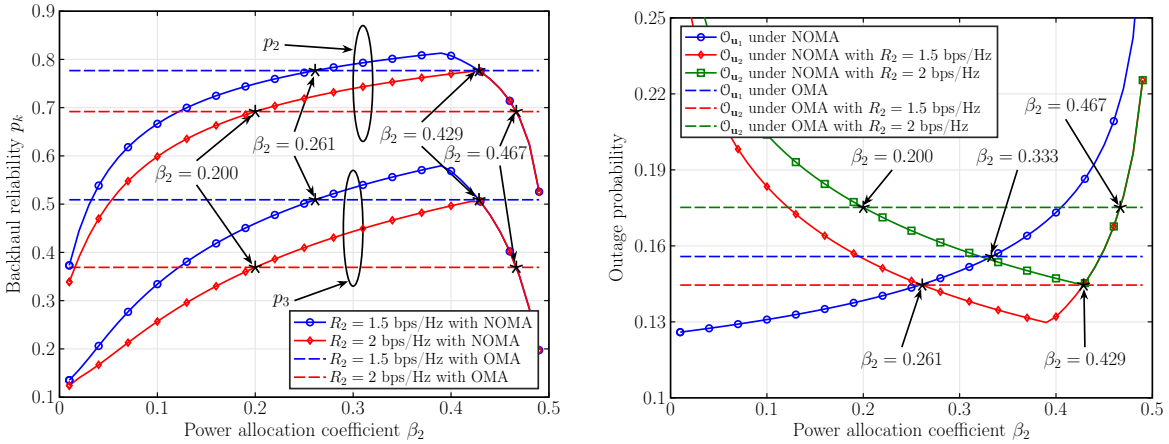

(a) Backhaul reliability comparison with $P_{\mathbf{b}} = 40$ dBm.

(b) Outage comparison with $P_{\mathbf{r}} = 37$ dBm and $\bar{p} = 0.9$.

Fig. 6. Backhaul reliability and outage probability vs. NOMA power allocation coefficient β_2 under various values of target rate R_2 for $\mathbf{u}_2$, with $P_{\mathbf{z}} = 37$ dBm, location set S_1, $\tilde{m}_k = \{4, 4, 2, 2\}$, and $R_1 = 1$ bps/Hz.

that the lower and higher limits of β_2 are determined by R_1 and R_2 and are the same for different links. This result will justify Corollary 4.

In Fig. 6b, the advantage of NOMA is studied in the aspect of outage probability with fixed $\bar{p} = 0.9$ and $P_{\mathbf{r}} = 37$ dBm. To guarantee a lower outage probability for $\mathbf{u}_1$, β_2 should be lower than $\frac{1}{2^{R_1}+1}$. On one hand, the transmit power for $\mathbf{u}_1$ decreases due to the power splitting of the NOMA protocol. On the other hand, $\mathbf{u}_1$ is decoded before $\mathbf{u}_2$, so the signal of $\mathbf{u}_2$ will interfere with the signal reception at $\mathbf{u}_1$. As for $\mathcal{O}_{\mathbf{u}_2}$, similar observation can be obtained as in Fig. 6a that, to guarantee the superiority of NOMA, the condition of $\frac{1}{2^{R_2}+1} < \beta_2 < \frac{2^{2R_2-R_1}-1}{2^{2R_2}-1}$ should be satisfied. Thus, we can see that at the same amount of resource blocks, OMA requires a much higher SINR than NOMA to guarantee the same overall target rate. This is another justification of Corollary 4.

We also illustrate the advantage of NOMA over OMA in Fig. 7 in terms of the outage sum rate and energy efficiency.

In Fig. 7a, the outage sum rates are plotted under the same system parameter settings as those in Fig. 6b. Besides the design insight in β_2, another conclusion can be drawn that with a high target rate R_2, NOMA takes obvious advantage over OMA in the aspect of outage sum rate. However, this superiority of NOMA will diminish in low target rate region.

In Fig. 7b, we fix the active probability of each ABS as $\bar{p} = 0.9$ and the power of the interfering nodes as $P_{\mathbf{z}} = 20$ dBm to study the energy efficiency, which is defined as the ratio

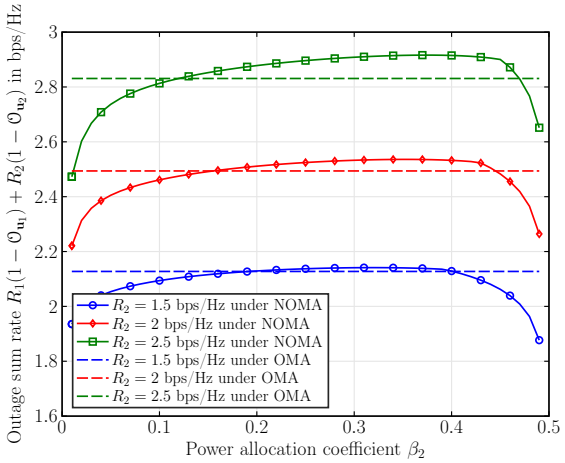

(a) Outage sum rate comparison under the same system parameter setting as those of Fig. 6b.

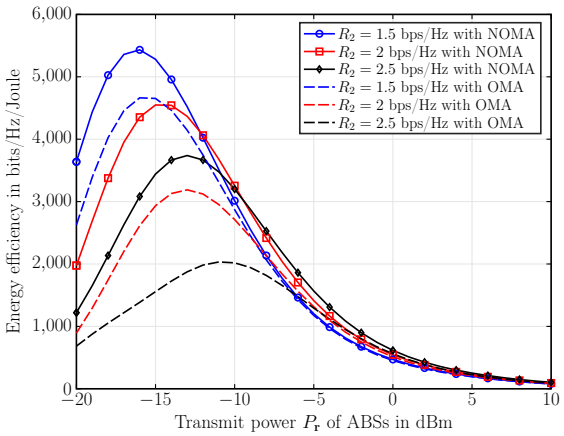

(b) Energy efficiency comparison with $R_2 = 4$ bps/Hz, $K = 2$, $\bar{p} = 0.9$, and $P_{\mathbf{z}} = 20$ dBm.

Fig. 7. Outage sum rate vs. power allocation coefficient β_2 and energy efficiency vs. transmit power $P_{\mathbf{r}}$ with target rate $R_1 = 1$ bps/Hz, location set S_1, and $\tilde{m}_k = \{4, 4, 2, 2\}$.

between the outage sum rate of the system, i.e., $R_1\left(1-\mathcal{O}_{\mathbf{u}_1}\right)+R_2\left(1-\mathcal{O}_{\mathbf{u}_2}\right)$, and the transmit power of all ABSs, i.e., $KP_{\mathbf{r}}$. The results are obtained under location set S_1 with $K = 2$ and the target rate for $\mathbf{u}_1$ fixed at $R_1 = 1$ bps/Hz.

Fig. 7b shows that NOMA can achieve a higher energy efficiency than OMA. However, when the transmit power is increased to a high level, the advantage will diminish gradually. This is because under the focused energy efficiency definition, the improvement in the outage sum rate is mainly due to the decrease in the outage probability. Since the target rates are fixed, a performance ceiling will limit the outage sum rate when the outage probability approaches zero. Thus, the energy efficiency will be the same for NOMA and OMA in the high transmit SNR region.

VI. Conclusion

In this paper, we have studied the system performance of an ABS-assisted network, where multiple ABSs were deployed to relay the downlink signals from the MBS to the UEs. We have considered cooperative signal transmissions, in which active ABSs have utilized NC-JT to realize a coherent power combination at the UEs. To improve connectivity, NOMA has been also considered for both the wireless backhaul and the wireless access. The interfering nodes were modeled as a PPP in the infinite 2D plane, and tools from stochastic geometry were

applied to facilitate analytical derivations. We have assumed more realistic probabilistic LoS and NLoS propagations for both the A2G and G2G channels. Different from most other works, non-identical Nakagami-m fading has also been assumed. Upon applying several more practical assumptions, we have derived closed-form expressions for the outage probability of the system and have validated the results through Monte Carlo simulations. Numerical results had been obtained to study the impact of various parameters on the performance metrics. We have shown that the wireless backhaul reliability, ABS number, and target rates are key factors to determine the system performance. It has been shown that the ABS height should be carefully designed to achieve the lowest outage probability and highest outage sum rate under the probabilistic LoS A2G channel. We have also verified the advantage of the NOMA scheme by comparing its outage probability, outage sum rate, and energy efficiency with those of the basic OMA scheme. The comparisons have shown that improved system performance can be achieved with a properly selected NOMA power allocation coefficient.

APPENDIX A
PROOF OF LEMMA 1

Since $W_{\mathbf{r},\mathbf{u}_j} = \sum_{k=1}^{K} W_{\mathbf{r}_k,\mathbf{u}_j}\mathbb{I}_k$, we start by studying the CDF of $W_{\mathbf{r}_k,\mathbf{u}_j}\mathbb{I}_k$, which is given by

$$\begin{aligned} F_{W_{\mathbf{r}_k,\mathbf{u}_j}\mathbb{I}_k}(w) &= \mathbb{P}\left(W_{\mathbf{r}_k,\mathbf{u}_j}\mathbb{I}_k \le w\right) \\ &= \mathbb{P}\left(\mathbb{I}_k = 0\right)\mathbb{P}(0 \le w) + \mathbb{P}(\mathbb{I}_k = 1)\mathbb{P}\left(W_{\mathbf{r}_k,\mathbf{u}_j} \le w\right) = 1 - p_k + p_k F_{W_{\mathbf{r}_k,\mathbf{u}_j}}(w), \end{aligned} \quad (35)$$

where $F_{W_{\mathbf{r}_k,\mathbf{u}_j}}(w)$ is the CDF of $W_{\mathbf{r}_k,\mathbf{u}_j}$. Hence we have the probability density function (PDF) of $W_{\mathbf{r}_k,\mathbf{u}_j}\mathbb{I}_k$ derived as

$$f_{W_{\mathbf{r}_k,\mathbf{u}_j}\mathbb{I}_k}(w) = (1 - p_k)\delta(w) + p_k f_{W_{\mathbf{r}_k,\mathbf{u}_j}}(w), \quad (36)$$

where $f_{W_{\mathbf{r}_k,\mathbf{u}_j}}(w)$ is the PDF of $W_{\mathbf{r}_k,\mathbf{u}_j}$, and $\delta(\cdot)$ is the Dirac delta function satisfying $\int_{-\infty}^{\infty}\delta(t-\tau)f(t)\mathrm{d}t = f(\tau)$.

To obtain the CDF of $W_{\mathbf{r},\mathbf{u}_j}$, we firstly resort to the moment generating function (MGF) of $W_{\mathbf{r}_k,\mathbf{u}_j}\mathbb{I}_k$ given by

$$\begin{aligned} \mathcal{M}_{W_{\mathbf{r}_k,\mathbf{u}_j}\mathbb{I}_k}(s) &= \mathbb{E}_{W_{\mathbf{r}_k,\mathbf{u}_j}\mathbb{I}_k}\left[\exp\left(sW_{\mathbf{r}_k,\mathbf{u}_j}\mathbb{I}_k\right)\right] = \int_0^{\infty}\exp(sw)f_{W_{\mathbf{r}_k,\mathbf{u}_j}\mathbb{I}_k}(w)\mathrm{d}w \\ &= (1-p_k)\underbrace{\int_0^{\infty}\exp(sw)\delta(w)\mathrm{d}w}_{\exp(s\cdot 0)=1} + p_k\underbrace{\int_0^{\infty}\exp(sw)f_{W_{\mathbf{r}_k,\mathbf{u}_j}}(w)\mathrm{d}w}_{\text{the MGF of } W_{\mathbf{r}_k,\mathbf{u}_j}} \\ &\overset{(a)}{=} 1 - p_k + p_k\left(\mathrm{P}_{\mathrm{AN}}\left(D_{k,j}\right)\left(1 - s\vartheta_{k,j}\right)^{-1} + \mathrm{P}_{\mathrm{AL}}\left(D_{k,j}\right)\left(1 - s\theta_{k,j}\right)^{-m_{k,j}}\right), \end{aligned} \quad (37)$$

$$\begin{aligned}
\mathcal{M}_{W_{\mathbf{r},\mathbf{u}_j}}(s) &= \mathbb{E}\left[\exp\left(s\sum_{k=1}^{K} W_{\mathbf{r}_k,\mathbf{u}_j}\mathbb{I}_k\right)\right] = \prod_{k=1}^{K}\mathcal{M}_{W_{\mathbf{r}_k,\mathbf{u}_j}\mathbb{I}_k}(s) \\
&= \prod_{k=1}^{K}\left((1-p_k)+p_k\left(\mathrm{P}_{\mathrm{AN}}\left(D_{k,j}\right)\left(1-s\vartheta_{k,j}\right)^{-1}+\mathrm{P}_{\mathrm{AL}}\left(D_{k,j}\right)\left(1-s\theta_{k,j}\right)^{-m_{k,j}}\right)\right) \\
&= Q\prod_{k=1}^{K}\left(1+\frac{p_k}{1-p_k}\left(\underbrace{\mathrm{P}_{\mathrm{AN}}\left(D_{k,j}\right)\left(1-s\vartheta_{k,j}\right)^{-1}}_{A_k}+\underbrace{\mathrm{P}_{\mathrm{AL}}\left(D_{k,j}\right)\left(1-s\theta_{k,j}\right)^{-m_{k,j}}}_{B_k}\right)\right) \\
&\overset{(b)}{=} Q\sum_{t_1=0}^{1}\cdots\sum_{t_K=0}^{1}\prod_{k=1}^{K}\left(\frac{p_k}{1-p_k}\right)^{t_k}\prod_{k=1}^{K}\left(A_k+B_k\right)^{t_k} \\
&\overset{(c)}{=} Q\sum_{t_1=0}^{1}\cdots\sum_{t_K=0}^{1}\prod_{k=1}^{K}\left(\frac{p_k}{1-p_k}\right)^{t_k}\sum_{a_1=0}^{t_1}\cdots\sum_{a_K=0}^{t_K}\prod_{k=1}^{K}A_k^{a_k}B_k^{t_k-a_k} \\
&= Q\sum_{t_1=0}^{1}\cdots\sum_{t_K=0}^{1}\prod_{k=1}^{K}\left(\frac{p_k}{1-p_k}\right)^{t_k}\sum_{a_1=0}^{t_1}\cdots\sum_{a_K=0}^{t_K}\prod_{k=1}^{K}\mathrm{P}_{\mathrm{AN}}^{a_k}\left(D_{k,j}\right)\mathrm{P}_{\mathrm{AL}}^{t_k-a_k}\left(D_{k,j}\right) \\
&\quad\times\underbrace{\prod_{k=1}^{K}\left(1-s\vartheta_{k,j}\right)^{-a_k}\left(1-s\theta_{k,j}\right)^{-m_{k,j}(t_k-a_k)}}_{J_{\mathcal{T}}}. \qquad (38)
\end{aligned}$$

where $\mathbb{E}_X[\cdot]$ is the expectation over X, and (a) follows directly from calculating the MGF of $W_{\mathbf{r}_k,\mathbf{u}_j}$, which is a probabilistic gamma or exponentially distributed random variable.

Hence the MGF of $W_{\mathbf{r},\mathbf{u}_j}$ can be obtained in (38), shown at the top this page, where (b) and (c) are expansions according to the multi-binomial theorem. Note that $\mathcal{J}_{\mathcal{T}}$ in (38) is in the form of partial fraction [33], and can be expanded as

$$\mathcal{J}_{\mathcal{T}} = \sum_{k=1}^{K}\left(\sum_{\nu=1}^{a_k}\eta_{k,j,\nu}\left(s-\frac{1}{\vartheta_{k,j}}\right)^{-\nu} + \sum_{\nu=1}^{m_{k,j}(t_k-a_k)}\mu_{k,j,\nu}\left(s-\frac{1}{\theta_{k,j}}\right)^{-\nu}\right), \qquad (39)$$

where $\eta_{k,j,\nu}$ is calculated in (40), shown at the top of the next page. Through some algebraic manipulations, we can reach the expression for $\eta_{k,j,\nu}$ provided in (16). The calculation of $\mu_{k,j,\nu}$ follows similar way as $\eta_{k,j,\nu}$, and is provided in (17).

$$\begin{aligned}\eta_{k,j,\nu} &= \frac{1}{(a_k-\nu)!}\left(-\frac{1}{\vartheta_{k,j}}\right)^{a_k}\left[\frac{\mathrm{d}^{a_k-\nu}}{\mathrm{d}s^{a_k-\nu}}\mathcal{J}_{\mathcal{T}}\cdot(1-s\vartheta_{k,j})^{a_k}\right]\Big|_{s\to\frac{1}{\vartheta_{k,j}}} \\ &= \frac{1}{(a_k-\nu)!}\left(-\frac{1}{\vartheta_{k,j}}\right)^{a_k}\sum_{\mathcal{Q}_{k,\nu}}\frac{(a_k-\nu)!}{\prod_{n=1,n\neq k}^{K}(q_n!)\prod_{n=1}^{K}(p_n!)} \\ &\quad\times\prod_{n=1,n\neq k}^{K}\left(\vartheta_{n,j}^{q_n}\frac{(a_n+q_n-1)!}{(a_n-1)!}\left[(1-\vartheta_{n,j}s)^{-a_n-q_n}\right]\Big|_{s\to\frac{1}{\vartheta_{k,j}}}\right) \\ &\quad\times\prod_{n=1}^{K}\left(\theta_{n,j}^{p_n}\frac{(m_{n,j}(t_n-a_n)+p_n-1)!}{(m_{n,j}(t_n-a_n)-1)!}\left[(1-\theta_{n,j}s)^{-m_{n,j}(t_n-a_n)-p_n}\right]\Big|_{s\to\frac{1}{\vartheta_{k,j}}}\right). \end{aligned} \tag{40}$$

By substituting (39) into (38), we can have that

$$\begin{aligned}\mathcal{M}_{W_{\mathbf{r},\mathbf{u}_j}}(s) &= Q\sum_{t_1=0}^{1}\cdots\sum_{t_K=0}^{1}\prod_{k=1}^{K}\left(\frac{p_k}{1-p_k}\right)^{t_k}\sum_{a_1=0}^{t_1}\cdots\sum_{a_K=0}^{t_K}\prod_{k=1}^{K}\mathrm{P}_{\mathrm{AN}}^{a_k}(D_{k,j})\,\mathrm{P}_{\mathrm{AL}}^{t_k-a_k}(D_{k,j}) \\ &\quad\times\sum_{k=1}^{K}\left(\sum_{\nu=1}^{a_k}\frac{\eta_{k,j,\nu}}{(-\vartheta_{k,j})^{-\nu}}(1-s\vartheta_{k,j})^{-\nu}+\sum_{\nu=1}^{m_k(t_k-a_k)}\frac{\mu_{k,j,\nu}}{(-\theta_{k,j})^{-\nu}}(1-s\theta_{k,j})^{-\nu}\right). \end{aligned} \tag{41}$$

Recall that $(1-s\theta)^{-\nu}$ is the MGF of a gamma distributed variable with shape parameter ν and scale parameter θ. Hence we can observe that (41) involves the weighted sum of the MGFs of several gamma distributed variables. This helps to reach the CDF of $W_{\mathbf{r},\mathbf{u}_j}$ in (15), which is in the form of the weighted sum of CDFs of several gamma distributed variables.

When the A2G channel degrades to deterministic LoS propagation model, we have the MGF of $\hat{W}_{\mathbf{r}_k,\mathbf{u}_j}$ calculated as

$$\mathcal{M}_{\hat{W}_{\mathbf{r}_k,\mathbf{u}_j}}(s) = 1-\hat{p}_k+\hat{p}_k\,(1-s\theta_{k,j})^{-m_{k,j}}\,, \tag{42}$$

and then the MGF of $\hat{W}_{\mathbf{r},\mathbf{u}_j}$ calculated as

$$\begin{aligned}\mathcal{M}_{\hat{W}_{\mathbf{r},\mathbf{u}_j}}(s) &= \prod_{k=1}^{K}\mathcal{M}_{\hat{W}_{\mathbf{r}_k,\mathbf{u}_j}\mathbb{I}_k}(s) = Q\prod_{k=1}^{K}\left(1+\frac{p_k}{1-p_k}(1-s\theta_{k,j})^{-m_{k,j}}\right) \\ &= Q\sum_{t_1=0}^{1}\cdots\sum_{t_K=0}^{1}\prod_{k=1}^{K}\left(\frac{p_k}{1-p_k}\right)^{t_k}\underbrace{\prod_{k=1}^{K}(1-\theta_{k,j})^{-m_{k,j}t_k}}_{\hat{\mathcal{J}}_{\mathcal{T}}}. \end{aligned} \tag{43}$$

Again, by partial fraction expansion, $\hat{\mathcal{J}}_{\mathcal{T}}$ can be rewritten into a weighted sum form as

$$\hat{\mathcal{J}}_{\mathcal{T}} = \sum_{k=1}^{K} \sum_{\nu=1}^{m_{k,j}t_k} \hat{\mu}_{k,j,\nu} \left(s - \frac{1}{\theta_{k,j}} \right)^{-\nu}, \tag{44}$$

where the calculation of $\hat{\mu}_{k,j,\nu}$ follows similar ways as $\eta_{k,j,\nu}$ and $\mu_{k,j,\nu}$. Then, the CDF of $\hat{W}_{\mathbf{r},\mathbf{u}_j}$ can be finally reached in (20).

APPENDIX B
PROOF OF THEOREM 1

We start the derivation under the general J-user case ($J \geq 2$) to extend our 2-user system model to multi-user scenarios. In such a general case, the SINR $\gamma_{\mathbf{r}_k,j}$ of s_j at $\mathbf{r}_k$ is calculated as

$$\gamma_{\mathbf{r}_k,j} = \frac{\beta_j W_{\mathbf{b},\mathbf{r}_k}}{I_{\mathbf{r}_k} + \sum_{\iota=j+1}^{J} \beta_\iota W_{\mathbf{b},\mathbf{r}_k} + 1}. \tag{45}$$

By definition, p_k is given by $p_k = \mathbb{P}\left(\gamma_{\mathbf{r}_k,1} \geq \epsilon_1, \cdots, \gamma_{\mathbf{r}_k,J} \geq \epsilon_J\right)$, and then we have

$$\begin{aligned}
p_k &= \mathbb{P}\left(\frac{\beta_1 W_{\mathbf{b},\mathbf{r}_k}}{I_{\mathbf{r}_k} + \sum_{\iota=2}^{J} \beta_\iota W_{\mathbf{b},\mathbf{r}_k} + 1} > \epsilon_1, \cdots, \frac{\beta_j W_{\mathbf{b},\mathbf{r}_k}}{I_{\mathbf{r}_k} + \sum_{\iota=j+1}^{J} \beta_\iota W_{\mathbf{b},\mathbf{r}_k} + 1} > \epsilon_j, \cdots, \frac{\beta_J W_{\mathbf{b},\mathbf{r}_k}}{I_{\mathbf{r}_k} + 1} > \epsilon_J \right) \\
&= \mathbb{P}\left(W_{\mathbf{b},\mathbf{r}_k} > \frac{\epsilon_1 \left(I_{\mathbf{r}_k} + 1\right)}{\beta_1 - \epsilon_1 \sum_{\iota=2}^{J} \beta_\iota}, \cdots, W_{\mathbf{b},\mathbf{r}_k} > \frac{\epsilon_j \left(I_{\mathbf{r}_k} + 1\right)}{\beta_j - \epsilon_j \sum_{\iota=j+1}^{J} \beta_\iota}, \cdots, W_{\mathbf{b},\mathbf{r}_k} > \frac{\epsilon_J \left(I_{\mathbf{r}_k} + 1\right)}{\beta_J} \right) \\
&= \mathbb{P}\left(W_{\mathbf{b},\mathbf{r}_k} > \xi_J \left(I_{\mathbf{r}_k} + 1\right) \right) = \bar{F}_{W_{\mathbf{b},\mathbf{r}_k}} \left(\xi_J \left(I_{\mathbf{r}_k} + 1\right) \right) \\
&= \mathrm{P}_{\mathrm{AN}}\left(\tilde{D}_k\right) \underbrace{\texttt{ExpCCDF}\left(\xi_J \left(I_{\mathbf{r}_k} + 1\right), \frac{1}{\vartheta_k} \right)}_{p_{k|\mathrm{N}}} + \mathrm{P}_{\mathrm{AL}}\left(\tilde{D}_k\right) \underbrace{\texttt{GamCCDF}\left(\xi_J \left(I_{\mathbf{r}_k} + 1\right), \tilde{m}_k, \theta_k \right)}_{p_{k|\mathrm{L}}},
\end{aligned} \tag{46}$$

where $\xi_j = \max\left\{ \frac{\epsilon_1}{\beta_1 - \epsilon_1 \sum_{\iota=2}^{J} \beta_\iota}, \cdots, \frac{\epsilon_j}{\beta_j - \epsilon_j \sum_{\iota=j+1}^{J} \beta_\iota} \right\}$ and the power allocation coefficient should satisfy $\beta_j > \epsilon_j \sum_{\iota=j+1}^{J} \beta_\iota$ for $1 \leq j \leq J$. Also note that (46) is composed of two conditional active probabilities $p_{k|\mathrm{N}}$ and $p_{k|\mathrm{L}}$. For $p_{k|\mathrm{N}}$, it can be derived as

$$\begin{aligned}
p_{k|\mathrm{N}} &= \mathbb{E}_{I_{\mathbf{r}_k}} \left[\exp\left(-\frac{\xi_J}{\vartheta_k} \left(I_{\mathbf{r}_k} + 1\right) \right) \right] = \exp\left(-\frac{\xi_J}{\vartheta_k} \right) \mathbb{E}_{I_{\mathbf{r}_k}} \left[\exp\left(-\frac{\xi_J}{\vartheta_k} I_{\mathbf{r}_k} \right) \right] \\
&= \exp\left(-\frac{\xi_J}{\vartheta_k} \right) \mathcal{L}_{I_{\mathbf{r}_k}} \left(\frac{\xi_J}{\vartheta_k} \right),
\end{aligned} \tag{47}$$

and the LT of $I_{\mathbf{r}_k}$ is calculated as

$$\mathcal{L}_{I_{\mathbf{r}_k}}(s) = \mathbb{E}\left[\exp\left(-s\sum_{\mathbf{z}_i\in\Phi}\rho_{\mathbf{z}}\zeta_{\mathbf{z}_i,\mathbf{r}_k}\right)\right] = \mathbb{E}_{\Phi}\left[\prod_{\mathbf{z}_i\in\Phi}\mathbb{E}_{\zeta_{\mathbf{z}_i,\mathbf{r}_k}}\left[\exp\left(-s\rho_{\mathbf{z}}\zeta_{\mathbf{z}_i,\mathbf{r}_k}\right)\right]\right]$$

$$\overset{(d)}{=} \mathbb{E}_{\Phi}\left[\prod_{\mathbf{z}_i\in\Phi}\mathbb{E}_{\tilde{Z}_{i,k},\tilde{g}_{i,k,\tilde{m}}}\left[\mathrm{P_{AN}}\left(\tilde{Z}_{i,k}\right)\exp\left(-s\rho_{\mathbf{z}}\tilde{Z}_{i,k}^{-\alpha_{\mathrm{N}}}\tilde{g}_{i,k,1}\right)+\mathrm{P_{AL}}\left(\tilde{Z}_{i,k}\right)\exp\left(-s\rho_{\mathbf{z}}\tilde{Z}_{i,k}^{-\alpha_{\mathrm{L}}}\tilde{g}_{i,k,\tilde{m}}\right)\right]\right]$$

$$\overset{(e)}{=} \mathbb{E}_{\Phi}\left[\prod_{\mathbf{z}_i\in\Phi}\mathbb{E}_{\tilde{Z}_{i,k}}\left[\frac{\mathrm{P_{AN}}\left(\tilde{Z}_{i,k}\right)}{1+s\rho_{\mathbf{z}}\tilde{Z}_{i,k}^{-\alpha_{\mathrm{N}}}}+\frac{\mathrm{P_{AL}}\left(\tilde{Z}_{i,k}\right)}{\left(1+\frac{s\rho_{\mathbf{z}}}{\tilde{m}}\tilde{Z}_{i,k}^{-\alpha_{\mathrm{L}}}\right)^{\tilde{m}}}\right]\right], \tag{48}$$

where (d) is due to the probabilistic LoS and NLoS A2G interference propagation, and (e) follows the MGF of exponential distribution and gamma distribution. Utilizing the probability generating functional (PGFL) of the PPP [36] and noting that the shortest distance from the ground interfering node to the ABS is h, (48) can be evaluated as (24).

For $p_{k|\mathrm{L}}$, it can be derived as

$$\begin{aligned}
p_{k|\mathrm{L}} &= \mathbb{E}_{I_{\mathbf{r}_k}}\left[\exp\left(-\frac{\xi_J}{\theta_k}\left(I_{\mathbf{r}_k}+1\right)\right)\sum_{l=0}^{\tilde{m}_k-1}\frac{1}{l!}\left(\frac{\xi_J}{\theta_k}\left(I_{\mathbf{r}_k}+1\right)\right)^l\right] \\
&= \exp\left(-\frac{\xi_J}{\theta_k}\right)\mathbb{E}_{I_{\mathbf{r}_k}}\left[\exp\left(-\frac{\xi_J}{\theta_k}I_{\mathbf{r}_k}\right)\sum_{l=0}^{\tilde{m}_k-1}\frac{1}{l!}\left(\frac{\xi_J}{\theta_k}\right)^l\sum_{\kappa=0}^{l}\binom{l}{\kappa}I_{\mathbf{r}_k}^{\kappa}\right] \\
&= \exp\left(-\frac{\xi_J}{\theta_k}\right)\sum_{l=0}^{\tilde{m}_k-1}\frac{1}{l!}\left(\frac{\xi_J}{\theta_k}\right)^l\sum_{\kappa=0}^{l}\binom{l}{\kappa}\mathbb{E}_{I_{\mathbf{r}_k}}\left[\exp\left(-\frac{\xi_J}{\theta_k}I_{\mathbf{r}_k}\right)\left(\frac{\xi_J}{\theta_k}I_{\mathbf{r}_k}\right)^{\kappa}\right] \\
&\overset{(f)}{=} \exp\left(-\frac{\xi_J}{\theta_k}\right)\sum_{l=0}^{\tilde{m}_k-1}\left(\frac{\xi_J}{\theta_k}\right)^l\sum_{\kappa=0}^{l}\binom{l}{\kappa}\frac{(-1)^{\kappa}}{l!}\mathcal{L}_{I_{\mathbf{r}_k}}^{(\kappa)}\left(\frac{\xi_J}{\theta_k}\right),
\end{aligned} \tag{49}$$

where (f) is due to the fact that $\mathbb{E}_I\left[I^{\kappa}\exp(-sI)\right] = (-1)^{\kappa}\mathcal{L}_I^{(\kappa)}(s)$, and $\mathcal{L}_I^{(\kappa)}(x_0) = \left[\frac{\mathrm{d}^{\kappa}}{\mathrm{d}s^{\kappa}}\mathcal{L}(s)\right]\Big|_{s=x_0}$ is the κ-th derivative of $\mathcal{L}_I(s)$ evaluated at $s=x_0$. To calculate $\mathcal{L}_I^{(\kappa)}(s)$, we resort to the Faà di Bruno formula to deal with the higher derivatives of composite function, which provides

$$f^{(\kappa)}(g(s)) = \sum_{(n_1,\cdots,n_\kappa)\in\mathcal{N}_\kappa}\frac{\kappa!}{\prod_{\tau=1}^{\kappa}(n_\tau!)}f^{(n_1+\cdots+n_\kappa)}(g(s))\prod_{\tau=1}^{\kappa}\left(\frac{g^{(\tau)}(s)}{\tau!}\right)^{n_\tau}. \tag{50}$$

Thus, we have

$$\begin{aligned}
\mathcal{L}_{I_{\mathbf{r}_k}}^{(\kappa)}(s) &= \sum_{(n_1,\cdots,n_\kappa)\in\mathcal{N}_\kappa}\frac{\kappa!}{\prod_{\tau=1}^{\kappa}(n_\tau!)}\mathcal{L}_{I_{\mathbf{r}_k}}(s) \\
&\times\prod_{\tau=1}^{\kappa}\left(2\pi\lambda\int_h^{\infty}\left(\frac{\mathrm{P_{AN}}(z)\left(-\rho_{\mathbf{z}}z^{-\alpha_{\mathrm{N}}}\right)^{\tau}}{\left(1+s\rho_{\mathbf{z}}z^{-\alpha_{\mathrm{N}}}\right)^{\tau+1}}+\binom{\tilde{m}-1+\tau}{\tilde{m}-1}\frac{\mathrm{P_{AL}}(z)\left(-\frac{\rho_{\mathbf{z}}}{\tilde{m}}z^{-\alpha_{\mathrm{L}}}\right)^{\tau}}{\left(1+\frac{s\rho_{\mathbf{z}}}{\tilde{m}}z^{-\alpha_{\mathrm{L}}}\right)^{\tau+\tilde{m}}}\right)z\mathrm{d}z\right)^{n_\tau}.
\end{aligned} \tag{51}$$

By setting $J=2$ and substituting (51) into (49) and then into (46), we finally reach the expression of p_k in (23).

REFERENCES

[1] S. Chandrasekharan, K. Gomez, A. Al-Hourani, *et al.*, "Designing and implementing future aerial communication networks," *IEEE Commun. Mag.*, vol. 54, no. 5, pp. 26–34, May 2016.

[2] Y. Zeng, R. Zhang, and T. J. Lim, "Wireless communications with unmanned aerial vehicles: Opportunities and challenges," *IEEE Commun. Mag.*, vol. 54, no. 5, pp. 36–42, 5 2016.

[3] H. Menouar, I. Güvenc, K. Akkaya, *et al.*, "UAV-enabled intelligent transportation systems for the smart city: Applications and challenges," *IEEE Commun. Mag.*, vol. 55, no. 3, pp. 22–28, Mar. 2017.

[4] M. Erdelj, E. Natalizio, K. R. Chowdhury, *et al.*, "Help from the sky: Leveraging UAVs for disaster management," *IEEE Pervasive Comput.*, vol. 16, no. 1, pp. 24–32, Jan. 2017.

[5] L. Wang, H. Yang, J. Long, *et al.*, "Enabling ultra-dense UAV-aided network with overlapped spectrum sharing: Potential and approaches," *IEEE Network*, vol. 32, no. 5, pp. 85–91, Sep. 2018.

[6] S. Sekander, H. Tabassum, and E. Hossain, "Multi-tier drone architecture for 5G/B5G cellular networks: Challenges, trends, and prospects," *IEEE Commun. Mag.*, vol. 56, no. 3, pp. 104–111, Mar. 2018.

[7] Z. Zhou, J. Feng, L. Tan, *et al.*, "An air-ground integration approach for mobile edge computing in IoT," *IEEE Commun. Mag.*, vol. 56, no. 8, pp. 40–47, Aug. 2018.

[8] R. Tanbourgi, S. Singh, J. G. Andrews, *et al.*, "A tractable model for noncoherent joint-transmission base station cooperation," *IEEE Trans. Wireless Commun.*, vol. 13, no. 9, pp. 4959–4973, Sep. 2014.

[9] M. Sami, N. K. Noordin, M. Khabazian, *et al.*, "A survey and taxonomy on medium access control strategies for cooperative communication in wireless networks: Research issues and challenges," *IEEE Commun. Surveys Tuts.*, vol. 18, no. 4, pp. 2493–2521, Nov. 2016.

[10] H. Zhang, Y. Qiu, K. Long, *et al.*, "Resource allocation in NOMA-based fog radio access networks," *IEEE Wireless Commun. Mag.*, vol. 25, no. 3, pp. 110–115, Mar. 2018.

[11] Z. Qin, X. Yue, Y. Liu, *et al.*, "User association and resource allocation in unified NOMA enabled heterogeneous ultra dense networks," *IEEE Commun. Mag.*, vol. 56, no. 6, pp. 86–92, Jun. 2018.

[12] X. Wang, H. Zhang, Y. Tian, *et al.*, "Modeling and analysis of aerial base station-assisted cellular networks in finite areas under LoS and NLoS propagation," *IEEE Trans. Wireless Commun.*, vol. 17, no. 10, pp. 6985–7000, Oct. 2018.

[13] N. Rupasinghe, Y. Yapıcı, İ. Güvenç, *et al.*, "Non-orthogonal multiple access for mmWave drone networks with limited feedback," *IEEE Trans. Commun.*, vol. 67, no. 1, pp. 762–777, Jan. 2019.

[14] Y. Zhu, G. Zheng, and M. Fitch, "Secrecy rate analysis of UAV-enabled mmWave networks using Matérn hardcore point processes," *IEEE J. Sel. Areas Commun.*, vol. 36, no. 7, pp. 1397–1409, Jul. 2018.

[15] M. Mozaffari, W. Saad, M. Bennis, *et al.*, "Mobile unmanned aerial vehicles (UAVs) for energy-efficient internet of things communications," *IEEE Trans. Wireless Commun.*, vol. 16, no. 11, pp. 7574–7589, Nov. 2017.

[16] J. Lyu, Y. Zeng, and R. Zhang, "Placement optimization of UAV-mounted mobile base stations," *IEEE Commun. Lett.*, vol. 21, no. 3, pp. 604–607, Mar. 2017.

[17] Y. Zeng and R. Zhang, "Energy-efficient UAV communication with trajectory optimization," *IEEE Trans. Wireless Commun.*, vol. 16, no. 6, pp. 3747–3760, Jun. 2017.

[18] K. J. Kim, M. D. Renzo, H. Liu, *et al.*, "Performance analysis of distributed single carrier systems with distributed cyclic delay diversity," *IEEE Trans. Commun.*, vol. 65, no. 12, pp. 5514–5528, Dec. 2017.

[19] Q. Cui, X. Yu, Y. Wang, *et al.*, "The SIR meta distribution in Poisson cellular networks with base station cooperation," *IEEE Trans. Commun.*, vol. 66, no. 3, pp. 1234–1248, Mar. 2018.

[20] H. Zhang, B. Wang, C. Jiang, *et al.*, "Energy efficient dynamic resource optimization in NOMA systems," *IEEE Trans. Wireless Commun.*, vol. 17, no. 9, pp. 5671–5683, Sep. 2018.

[21] Z. Ding, X. Lei, G. K. Karagiannidis, *et al.*, "A survey on non-orthogonal multiple access for 5G networks: Research challenges and future trends," *IEEE J. Sel. Areas Commun.*, vol. 35, no. 10, pp. 2181–2195, Oct. 2017.

[22] Y. Chen, N. Zhao, Z. Ding, *et al.*, "Multiple UAVs as relays: Multi-hop single link versus multiple dual-hop links," *IEEE Trans. Wireless Commun.*, vol. 17, no. 9, pp. 6348–6359, Sep. 2018.

[23] H. Wu, X. Tao, N. Zhang, *et al.*, "Cooperative UAV cluster-assisted terrestrial cellular networks for ubiquitous coverage," *IEEE J. Sel. Areas Commun.*, vol. 36, no. 9, pp. 2045–2058, Sep. 2018.

[24] M. Hua, Y. Wang, M. Lin, *et al.*, "Joint CoMP transmission for UAV-aided cognitive satellite terrestrial networks," *IEEE Access*, vol. 7, pp. 14 959–14 968, Feb. 2019.

[25] T. M. Nguyen, W. Ajib, and C. Assi, "A novel cooperative NOMA for designing UAV-assisted wireless backhaul networks," *IEEE J. Sel. Areas Commun.*, vol. 36, no. 11, pp. 2497–2807, Nov. 2018.

[26] W. Mei and R. Zhang, "Uplink cooperative NOMA for cellular-connected UAV," *IEEE J. Sel. Topics Signal Process.*, vol. 13, no. 3, pp. 644–656, Jun. 2019.

[27] K. J. Kim, P. V. Orlik, and T. A. Khan, "Performance analysis of finite-sized co-operative systems with unreliable backhauls," *IEEE Trans. Wireless Commun.*, vol. 15, no. 7, pp. 5001–5015, Jul. 2016.

[28] X. Wang, H. Zhang, Y. Tian, *et al.*, "Performance analysis of aerial base station assisted cooperative communication systems," in *Proc. IEEE Veh. Technol. Conf. (VTC'2019-Spring)*, Kuala Lumpur, Malaysia, Apr. 2019, pp. 1–5.

[29] A. A. Khuwaja, Y. Chen, N. Zhao, *et al.*, "A survey of channel modeling for UAV communications," *IEEE Commun. Surveys Tuts.*, vol. 20, no. 4, pp. 2804–2821, fourth quarter 2018.

[30] M. Ding, P. Wang, D. López-Pérez, *et al.*, "Performance impact of LoS and NLoS transmissions in dense cellular networks," *IEEE Trans. Wireless Commun.*, vol. 15, no. 3, pp. 2365–2380, Mar. 2016.

[31] H. Yu, I.-H. Lee, and G. L. Stüber, "Outage probability of decode-and-forward cooperative relaying systems with co-channel interference," *IEEE Trans. Wireless Commun.*, vol. 11, no. 1, pp. 266–274, Jan. 2012.

[32] Y. Liu, H. Xing, C. Pan, *et al.*, "Multiple-antenna-assisted non-orthogonal multiple access," *IEEE Wireless Commun. Mag.*, vol. 25, no. 2, pp. 17–23, Feb. 2018.

[33] I. S. Gradshteyn and I. M. Ryzhik, *Table of Integrals, Series, and Products*. Burlington, MA, USA: Academic Press, 2007.

[34] A. K. Gupta, H. S. Dhillon, S. Vishwanath, *et al.*, "Downlink multi-antenna heterogeneous cellular network with load balancing," *IEEE Trans. Commun.*, vol. 62, no. 11, pp. 4052–4067, Nov. 2014.

[35] D. W. Matolak and R. Sun, "Air-ground channel characterization for unmanned aircraft systems-part iii: The suburban and near-urban environments," *IEEE Trans. Veh. Technol.*, vol. 66, no. 8, pp. 6607–6618, Aug. 2017.

[36] S. Chiu, D. Stoyan, W. Kendall, *et al.*, *Stochastic Geometry and its Applications*. United Kingdom: John Wiley & Sons, Ltd, 2013.